# Buffer-Dependent Photophysics of 2-Aminopurine: Insights into Fluorescence Quenching and Excited-State Interactions

Souvik Poddar<sup>1,2</sup>, Marcia Levitus<sup>1,2,\*</sup>

- <sup>1</sup> School of Molecular Sciences, Arizona State University, 551 E. University Drive, Tempe, AZ, 85287, USA.
- <sup>2</sup> The Biodesign Institute Center for Single Molecule Biophysics, Arizona State University, Tempe, AZ, 85287, USA.
- \* To whom correspondence should be addressed: **ML** Tel: +1-480-727-8586; Fax: +1-480-727-2378; Email: marcia.levitus@asu.edu

#### **ABSTRACT**

2-Aminopurine (2AP) is the most widely used fluorescent nucleobase analog in DNA and RNA research. Its unique photophysical properties and environmental sensitivity make it an effective reporter of local environmental changes, thereby offering valuable molecular insights into nucleic acid dynamics and DNA-protein interactions. We studied the effect of ions present in commonly used buffer solutions (phosphate, carbonate, TRIS, HEPES, MOPS) on the excited-state photophysical properties of 2AP. Fluorescence quenching was significant for all buffers except TRIS. Results indicate that the two tautomers of 2AP (7H, 9H) are quenched by phosphate ions to different extents. Quenching by the  $H_2PO_4^-$  ion is more pronounced for the 7H tautomer, while the opposite is true for the  $HPO_4^{2-}$  ion. For phosphate ions, the results of the time-resolved fluorescence study cannot be explained using a simple collisional quenching mechanism. Instead, results are consistent with transient interactions between 2AP and the phosphate ions. We postulate that excited-state interactions between the 2AP tautomers and a H-bond acceptor (phosphate, carbonate) result in significant quenching of the singlet-excited state of 2AP. Such interactions manifest in bi-exponential fluorescence intensity decays with pre-exponential factors that vary with quencher concentration, and downward curvatures of the Stern-Volmer plots.

#### 1. INTRODUCTION

The study of nucleic acid dynamics and interactions at the molecular level is crucial for understanding biological processes, from DNA replication and transcription to genetic mutations and repair mechanisms. Among the myriad of tools available for these investigations, 2-aminopurine (2AP, Fig. 1) stands out as the most widely used fluorescent nucleobase analog in DNA and RNA research.<sup>1,2</sup> Unlike the canonical DNA bases, which have excited-state lifetimes of the order of picoseconds and very low fluorescence quantum yields, 3.4 2AP is a bright fluorescent probe when free in solution. The high fluorescence quantum yield of free 2AP  $(\phi = 0.68)^1$  is significantly reduced when the probe is incorporated into nucleic acids due to interactions with the neighboring bases. 1,5 The unique photophysical properties of 2AP and its pronounced environmental sensitivity make it an effective reporter of local environmental changes, thereby offering valuable molecular insights into nucleic acid dynamics and DNA-protein interactions. 1,2,6-12 However, potential interactions of 2AP with other nucleobases, ions, and biomolecules can influence its photophysical responses, presenting further layers of complexity. One such significant factor is the potential quenching of the excited singlet state of 2AP by proximal molecules or ions. Quenching phenomena can drastically alter the fluorescence quantum yield and lifetime of the fluorophore, and this can lead to misinterpretations in fluorescence-based studies where 2AP is employed as a probe. Thus, characterizing fluorescence quenching phenomena has profound consequences for experimental design and data interpretation. Additionally, the study of fluorescence quenching may provide insights into the nature of molecular interactions, and given that phosphate groups are ubiquitous in biochemistry, understanding the interactions between phosphate ions and nucleobases carry implications that extend beyond just quenching considerations.

The excited-state properties of 2-amino purine has been the subject of numerous experimental and computational studies. <sup>13,14</sup> 2AP has been long assumed to be intrinsically fluorescent in aqueous solution, and quenched within nucleic acids by interactions with neighboring bases. <sup>1,5</sup> However, more recent measurements of jet-cooled 2AP-water clusters have shown that isolated (non-hydrated) 2AP is essentially non-fluorescent. The *c.a.* 150 ps lifetime of isolated 2AP increases by up to two orders of magnitude by solvating the molecule with a single water molecule, and the magnitude of this increase depends strongly on the specific hydrogen-bonding site with which the water molecule interacts. <sup>15</sup> Recognizing the pronounced susceptibility of 2AP to hydration and distinct hydrogen-bond configurations, we hypothesized that its interactions with ions that can serve as hydrogen-bond acceptors, might lead to significant effects in its emission properties. Consistent with this observation, Paterson et al. noted that the fluorescence of 2AP is markedly quenched in phosphate buffer relative to water. <sup>16</sup> Yet, given the different emphasis of their study, this finding was touched upon without an extensive examination.

In this research, we delved into the quenching effects of 2AP by ions that constitute buffer solutions widely used in nucleic acid studies. We placed particular focus on phosphate ions, not just because of the common use of phosphate buffers in research, but also due to their widespread role in biological systems. Fluorescence quenching was significant in phosphate, carbonate, HEPES, and MOPS buffers, and negligible in dilute TRIS. The analysis of the time-resolved fluorescence data at various emission wavelengths and phosphate concentrations reveals the presence of two tautomers of 2AP that are quenched by the phosphate ions to different extents. The experimental results cannot be interpreted on the basis of a simple collisional quenching mechanism. Instead, results are consistent with transient interactions between the excited state of 2AP and the phosphate ions that manifest in bi-exponential fluorescence

intensity decays with pre-exponential factors that vary with quencher concentration. The differences between 2AP and 2APr (Fig. 1), together with the fact that quenching was observed in phosphate and carbonate buffers, but not in solutions of sodium sulfate, suggest that interactions involve the formation of hydrogen bonds with the quencher acting as an H-bond acceptor.

**Figure 1.** Chemical structures of adenine (shown as the 9H tautomer), 2-aminopurine riboside (2APr), and the 9H and 7H tautomers of 2-aminopurine (2AP)

#### 2. EXPERIMENTAL SECTION

#### 2.1 Materials and Sample Preparation

2-amino purine (2AP, Millipore Sigma #A3509-100MG) and 2-amino purine riboside (2APr, AstaTech #F12889) were used as received. The DNA sample was prepared by annealing the following DNA strands purchased from IDT (IA, USA): 5'-CTA TGT TGG AAG CTT GCA ATT ATG ACT CTG TAC ACG AAG 3' and 5' CTT CGT GTA CAG AGT CAT A2APT TGC AAG CTT CCA ACA TAG 3'. The characters in bold face indicate the 2AP modification and the thymine positioned opposite to it. The source of all other chemicals and protocols for buffer preparation and DNA annealing are provided in the Supporting Information file. All buffers were prepared in freshly double distilled water and the pH of all solutions was measured before all measurements. Stock solutions of 2AP and 2APr with an absorbance of *c.a.* 2 at 315 nm were made fresh less than 24 h before being used in an experiment. The samples used for fluorescence quantum yield and fluorescence lifetime determinations were prepared by diluting the stock solution of 2AP or 2APr to an absorbance of ~0.05 in the desired buffer. Experiments in water at various pH values were performed in solutions prepared by adding 1M HCl or 1M NaOH to water to achieve the desired pH.

#### 2.2 Absorption, Excitation and Emission Spectra

Absorption spectra were measured in a dual-beam Shimadzu UV-1900i spectrophotometer. Steady-state excitation and emission fluorescence spectra were acquired on a PTI Quantamaster 4/2005SE spectrofluorimeter. Fluorescence spectra showed small contributions from Raman scattering at 352 nm, which were corrected by using the signal measured with water or a buffer sample as a blank in all other measurements.<sup>17</sup> Excitation spectra were corrected in real time for variations in lamp intensity. The absorbance of all solutions was kept at ~0.05 at the excitation wavelength to avoid inner filter effects.<sup>18</sup>

#### 2.3 Fluorescence Quantum Yield Determinations

Relative fluorescence quantum yields ( $\phi$ ) were determined as described previously<sup>18</sup> using 2AP in pure water as a reference ( $\phi$  = 0.68).<sup>1</sup> The excitation wavelength was 315 nm and the emission spectrum was measured and integrated in the 320-600 nm range. The absorbance of all solutions was kept at ~0.05 at the excitation wavelength. The fluorescence quantum yield was calculated as:

$$\phi^{S} = \phi^{R} \times \frac{\int_{0}^{\infty} I_{F}^{S}(\lambda_{em}) d\lambda_{em}}{\int_{0}^{\infty} I_{F}^{R}(\lambda_{em}) d\lambda_{em}} \times \frac{\left(1 - 10^{-A^{R}}\right)}{\left(1 - 10^{-A^{S}}\right)}$$

where the superscripts S and R refer to the sample and reference, respectively, A is the absorbance of the solution at the excitation wavelength, and  $I_F(\lambda_{em})$  is the emission wavelength-dependent fluorescence intensity. The values of  $\varphi$  are reported with an uncertainty of 3% or lower.

#### 2.4 Time Resolved Fluorescence

Time-resolved fluorescence intensity measurements were performed using the time-correlated singlephoton counting (TCSPC) technique as described elsewhere.<sup>18</sup> Details of the instrumental setup are provided in the Supporting Information file. The polarization of the emission was 54.7° relative to that of the excitation (magic angle conditions), and the instrumental response function (IRF, FWHM  $\approx$  40 ps) was determined from the scattering of a Ludox sample at 310 nm. For all experiments summarized in Figs. 2 and 3, the excitation and emission wavelengths were set at 310 nm and 380 nm, respectively. The fitting parameters were obtained through iterative reconvolution of the model function  $F(\lambda, t) =$  $F_0(\lambda) \sum_{i=1}^n \alpha_i(\lambda) e^{-t/\tau_i}$  (n = 1 or 2) with the measured IRF using a software package written in-house (ASUFIT). For the data summarized in Tables 2-4, signals were acquired by performing sequential measurements at seven  $\lambda_{em}$  values in the 350–410 nm range. The seven curves were simultaneously fitted using the global analysis feature of ASUFIT. The algorithm uses the measured IRF for all fluorescence decays, and assumes wavelength-independent lifetimes and wavelength-dependent amplitudes. For measurements using DNA samples (Fig. 4), measurements were performed using two different time resolutions (3.3 ns and 25 ns) and three emission wavelengths (380, 390, and 400 nm). Details of the analysis of these data are provided in a previous publication. 18 Briefly, the decay was fitted with four exponential terms. The two different time resolutions allow for a more accurate determination of the short (< 0.5 ns) and long (> 0.5 ns) lifetimes, and the global analysis of the curves measured at the different emission wavelengths minimizes the problem of correlation between pre-exponential factors and lifetimes, which is common when fitting multi-exponential decays.<sup>1</sup>

#### 3. RESULTS

## 3.1 Effect of pH on 2AP and 2APr fluorescence

Absorption and emission spectra, fluorescence lifetimes, and fluorescence quantum yields, were measured in water at various pH values by adjusting the pH with HCl or NaOH. These experiments were performed with the primary objective of disentangling the effect of pH from any potential specific effects arising from buffer components. The obtained results, summarized in Fig. S1 and Table S1 in the Supporting Information file, reveal that changes in the pH within the range of 5 to 9 had a negligible impact on the measured absorption and emission spectra, fluorescence lifetimes and fluorescence quantum yields. A

decrease in fluorescence quantum yield was observed in acidic conditions (Table S1), consistent with the protonation of the N1 position of 2AP (pK<sub>a</sub> = 3.3)<sup>19</sup>. Significant quenching was also observed at high pH values (pH > 11), which can be attributed to the deprotonation of the N9H or N7H sites (pK<sub>a</sub>(N<sub>9</sub>H) = 9.8 for adenine<sup>20</sup>). All fluorescence decays ( $\lambda_{exc}$  = 310 nm,  $\lambda_{em}$  = 380 nm) could be satisfactorily fitted with a single exponential term except for pH = 3, which required three exponential terms (Table S1). Collectively, these findings support the assumption that any observed variations in the spectral or photophysical properties of 2AP when dissolved in buffer solutions within a pH range of 5-9 can be attributed to specific interactions with the buffer components.

# 3.2 Quenching of 2AP and 2APr fluorescence in aqueous buffers

The addition of NaCl to water had a negligible effect on the fluorescence lifetime and fluorescence quantum yield of 2AP (Table S2). In stark contrast, measurements in various buffer solutions commonly used in nucleic acid research showed that buffer components can significantly quench 2AP fluorescence (Fig. 2 and Tables S3 and S4). Stern-Volmer constants ( $K_{SV}$ ) were determined from the slopes of the linear regression lines of the plots of Fig. 2. Among the studied buffers, the lowest quenching constant ( $K_{SV} = 0.70$  M<sup>-1</sup>) was measured for TRIS-Cl pH 7.5. Although this value is small (a 7% decrease in fluorescence intensity is expected at [TRIS] = 100 mM, it is still significant if free 2AP or 2APr are used as a fluorescence standard to determine relative fluorescence quantum yields of 2AP incorporated into nucleic acids. Significant quenching was observed across all other buffers examined in this study, including phosphate (pH 5, 7 and 9), carbonate (pH 10), MOPS (pH 7), and HEPES (pH 7). The highest quenching constants were measured for carbonate and phosphate buffers, and notably, these buffers also induced a small red-shift in the fluorescence spectrum of 2AP that was not observed for TRIS, MOPS, and HEPES (see Figs. S2 and S3). Quenching was negligible when 2AP was dissolved in solutions of Na<sub>2</sub>SO<sub>4</sub> at concentrations as high as 1M.

Measurements conducted in phosphate buffer (pH 7) revealed significant quenching effects, corroborating earlier findings by Paterson et al.<sup>16</sup> Fluorescence decays could be fitted with a single exponential term with a lifetime that exhibited a significant reduction with increasing phosphate concentration (Fig. 2C and table S4). Stern-Volmer plots displayed a linear relationship up to approximately 500 mM phosphate, followed by a downward curvature at higher quencher concentration. We note that these deviations were not reported in the earlier paper by Paterson et al. because of the smaller phosphate concentration range (≤ 100 mM) used in the study. As explained in depth in the discussion section, the observed curvature might be indicative of transient effects in fluorescence quenching due to 2AP-phosphate interactions in the excited state. However, a number of reports suggest that the  $H_2PO_4^-$  and  $HPO_4^{2-}$  ions may potentially selfassociate at these elevated concentrations, 21-24 introducing an added layer of complexity to the interpretation of the Stern-Volmer plots. Examination of the data at phosphate concentrations equal to or lower than 500 mM shows that the Stern-Volmer plots constructed from fluorescence intensities and fluorescence lifetimes are linear and overlap. These results, along with the bimolecular quenching constant ( $k_q = K_{SV}/\tau_0 = 1.1 \times 10^9 \,\text{M}^{-1}.\text{s}^{-1}$ ) derived from the slope of the Stern-Volmer plot ( $K_{SV} = 0.56 \,\text{M}^{-1}$ ) and the fluorescence lifetime measured in the absence of quencher ( $\tau_0$  = 11.8 ns), agree with the dynamic quenching mechanism previously described by Paterson et al. 16

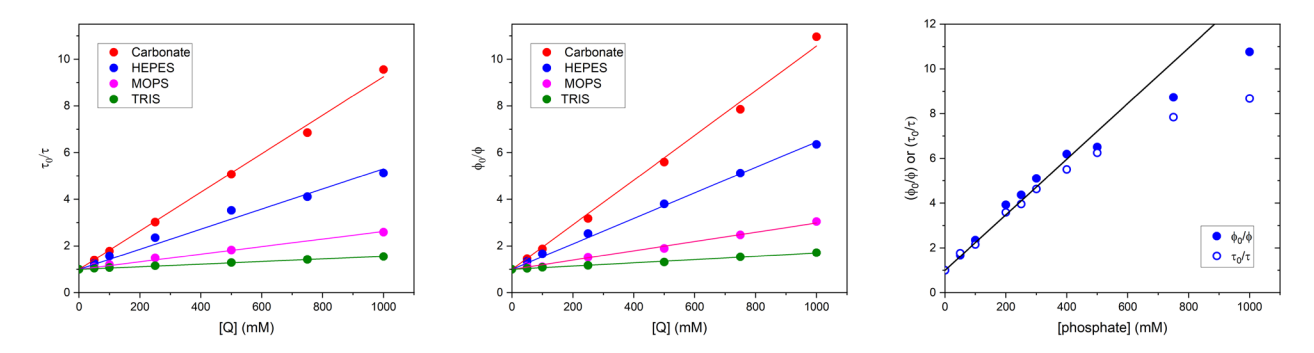


**Figure 2. A)** Quenching of 2AP by buffer components as observed by fluorescence lifetimes.  $τ_0$  refers to the fluorescence lifetime measured in the absence of quencher. Stern-Volmer constants are  $K_{sv} = 8.3 \text{ M}^{-1}$  (carbonate, red symbols),  $K_{sv} = 4.3 \text{ M}^{-1}$  (HEPES, blue symbols),  $K_{sv} = 1.6 \text{ M}^{-1}$  (MOPS, magenta symbols), and  $K_{sv} = 0.56 \text{ M}^{-1}$  (TRIS, green symbols). **B)** Quenching of 2AP by buffer components as observed by fluorescence quantum yields.  $φ_0$  refers to the fluorescence quantum yield measured in the absence of quencher. Stern-Volmer constants are  $K_{sv} = 9.6 \text{ M}^{-1}$  (carbonate, red symbols),  $K_{sv} = 5.5 \text{ M}^{-1}$  (HEPES, blue symbols),  $K_{sv} = 2.0 \text{ M}^{-1}$  (MOPS, magenta symbols), and  $K_{sv} = 0.70 \text{ M}^{-1}$  (TRIS, green symbols). **C)** Quenching of 2AP by phosphate buffer (pH 7). The solid line The Stern-Volmer constant calculated from fluorescence quantum yields at [phosphate]  $\le 500 \text{ mM}$  (solid line) is 12.5 M<sup>-1</sup>.

Reports of fluorescence quenching by MOPS and HEPES are scarce. We were only able to find one publication by Werner et al., who reported the collisional quenching of a zwitterionic biacridine derivative by both MOPS and HEPES.<sup>25</sup> Fluorescence quenching by phosphates, in contrast, has been reported for tyrosine,<sup>26-28</sup> tryptophan,<sup>29</sup> and other organic molecules.<sup>30-32</sup> Nevertheless, the phenomenon of fluorescence quenching induced by phosphates is rare when compared to widely recognized quenchers like acrylamide, iodide, or dabcyl. Moreover, within the group of fluorophores for which quenching by phosphate ions has been documented, the precise mechanistic underpinnings remain ambiguous, thus questioning whether a uniform mechanism exists, or whether there are variations on a case-by-case basis. The significant quenching effects observed in the experiments outlined above, coupled with the ubiquitous presence of phosphates in biological systems, motivated us to further investigate the influence of phosphates on 2AP fluorescence. Details of this analysis are provided in the next sections.

# 3.3 Quenching of 2AP and 2APr fluorescence by $H_2PO_4^-$ and $HPO_4^{2-}$

The experiments described above were repeated in phosphate buffers of pH 5 and 9, where the primary phosphate species are  $H_2PO_4^-$  and  $HPO_4^{2-}$ , respectively. A small but noticeable red-shift was observed in the emission spectra of 2AP and 2APr in phosphate buffer at both pH values (Fig. S2). As observed at pH 7, the analysis of the data shows that the Stern-Volmer plots constructed from fluorescence intensities are linear (Fig. 3). For 2AP, while the intensity decays acquired at pH 5 could be fitted with a single exponential term across all phosphate concentrations, decays measured at pH 9 required two exponential terms at phosphate concentrations greater than 50 mM (Table. S4 and Fig. S4). At pH 5, where all decays were monoexponential, the Stern-Volmer plots constructed from lifetimes showed a good overlap with the intensity data (Fig. 3). A similar result was observed at pH 9 at phosphate concentrations lower than approximately 400 mM if using the amplitude average lifetimes ( $\langle \tau \rangle = a_1\tau_1 + (1-a_1)\tau_2$ ) for the calculation of  $\tau_0/\tau$ . The bimolecular quenching constants calculated from the slopes of the intensity plots were determined as  $k_q = 8.6 \times 10^8 \, \text{M}^{-1}.\text{s}^{-1}$  (pH = 5) and  $1.1 \times 10^9 \, \text{M}^{-1}.\text{s}^{-1}$  (pH = 9). These findings indicate that the  $HPO_4^{2-}$  anion is a more efficient quencher of 2AP fluorescence than  $H_2PO_4^{-1}$ . As shown in Fig.3, this difference is more significant for the riboside, 2APr, where  $k_q = 6.8 \times 10^8 \, \text{M}^{-1}.\text{s}^{-1}$  (pH = 5) and  $1.2 \times 10^9 \, \text{M}^{-1}$ .

 $^{1}$ .s $^{-1}$ (pH = 9). All 2APr fluorescence decays could be fitted with a single exponential term at both pH values and across all phosphate concentrations.

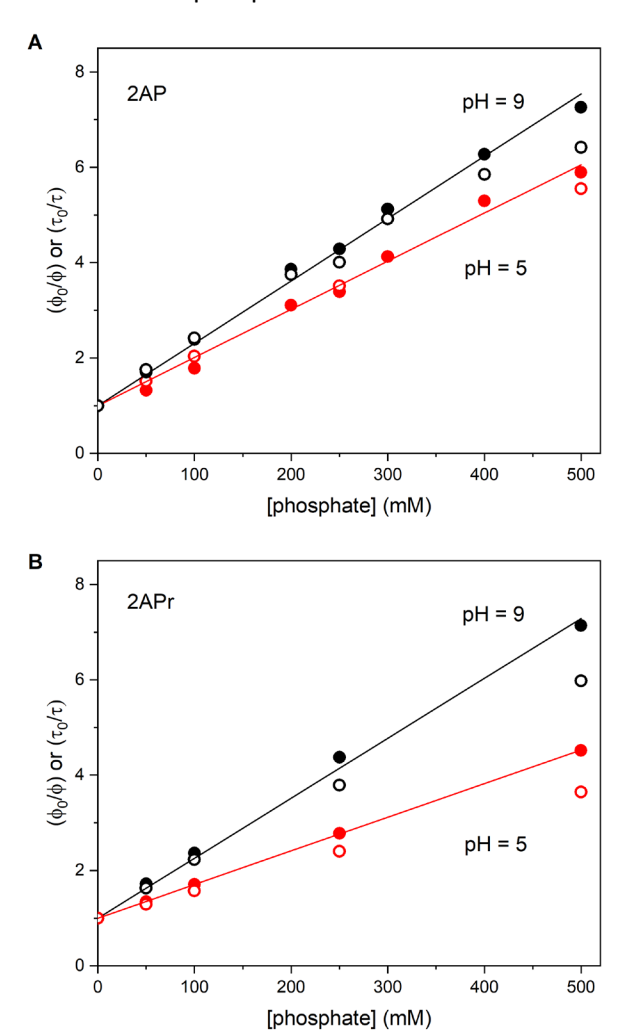


**Figure 3. A)** Quenching of 2AP by phosphate buffer at pH 5 (red) and pH 9 (black) as observed by fluorescence quantum yields (solid symbols) and fluorescence lifetimes (open symbols). Amplitude average lifetimes ( $\langle \tau \rangle = a_1\tau_1 + (1-a_1)\tau_2$ ) were used for the data acquired at pH 9 and [phosphate]  $\geq$  100 mM.  $\phi_0$  and  $\tau_0$  refer to the fluorescence quantum yield and fluorescence lifetime measured in the absence of phosphate, respectively. Solid lines represent fits to the  $\phi_0/\phi$  data. The bimolecular quenching constants calculated from the slopes of the intensity plots are  $k_q = 8.6 \times 10^8 \, \text{M}^{-1}.\text{s}^{-1} (\text{pH} = 5)$  and  $1.1 \times 10^9 \, \text{M}^{-1}.\text{s}^{-1} (\text{pH} = 9)$ . **B)** Results for 2APr. All fluorescence decays were monoexponential. The bimolecular quenching constants calculated from the slopes of the intensity plots are  $k_q = 6.8 \times 10^8 \, \text{M}^{-1}.\text{s}^{-1} (\text{pH} = 5)$  and  $1.2 \times 10^9 \, \text{M}^{-1}.\text{s}^{-1} (\text{pH} = 9)$ .

# 3.4 Quenching of 2AP incorporated into duplex DNA

When incorporated into DNA, 2AP fluorescence is quenched strongly by interactions with its neighboring bases.<sup>8,9,33-35</sup> Inter-base interactions in duplex DNA give rise to a multiexponential decay that reflects the highly heterogeneous environment sensed by the probe.<sup>6-9,36</sup> We measured the intensity decay of a 39 bp dsDNA sample containing a single 2AP modification (see Materials and Methods). Consistent with previous

reports, four exponential terms with lifetimes ranging from tens of picoseconds to nanoseconds were needed to fit the time-resolved fluorescence intensity decay (Table 1).35 Each lifetime represents a distribution of conformations in which 2AP experiences a similar environment, from more stacked (shortest lifetime), to more exposed to water (longest lifetime). The results are shown in Table 1, and the Stern-Volmer plots for the three longest lifetimes  $(\tau_2 - \tau_4)$  are shown in Fig. 4. The shortest lifetime  $(\tau_1 \approx$ 10-25 ps) fell below the resolution of the experiment (~30 ps) and could not be determined with the precision required to construct such a plot. Quenching was more significant for τ<sub>4</sub>, the longest lifetime, and negligible for  $\tau_2$ . This result is consistent with the interpretation that the longest lifetime ( $\tau_4$ ) arises from the small population of 2AP molecules that is more exposed to the solvent. Yet, the downward curvature of the Stern-Volmer plot, and the fact that quenching of  $\tau_4$  is less efficient than quenching of free 2AP in phosphate buffer at pH 7 (solid line in Fig. 4), indicate that the fraction of 2AP molecules that contribute to  $\tau_4$  is not fully accessible to the quencher. The curvature is more prominent for  $\tau_3$ , which arises from a fraction of 2AP molecules less exposed to the solvent relative to the population captured by  $\tau_4$ . The fraction of 2AP molecules that contribute to  $\tau_2$  is not accessible to the quencher. Although the presence of phosphate ions in the buffer had a minimal effect on the average fluorescence lifetime of 2AP incorporated into dsDNA, these results indicate that caution should be used when interpreting the individual lifetime components of 2AP to assess DNA conformation and dynamics in biophysical research.

Table 1. Effect of phosphate concentration on the fluorescence lifetimes of 2AP incorporated into duplex DNA.

[phosphate] (mM)	τ <sub>1</sub> (ns)	$\alpha_1$	τ <sub>2</sub> (ns)	$\alpha_2$	τ <sub>3</sub> (ns)	$\alpha_3$	τ <sub>4</sub> (ns)	α4
0	0.010	0.65	0.37	0.21	1.0	0.13	5.5	0.0079
20	0.018	0.66	0.39	0.20	0.92	0.13	4.8	0.0058
50	0.021	0.70	0.38	0.18	0.90	0.12	4.3	0.0060
100	0.026	0.66	0.38	0.21	0.89	0.12	4.0	0.0069

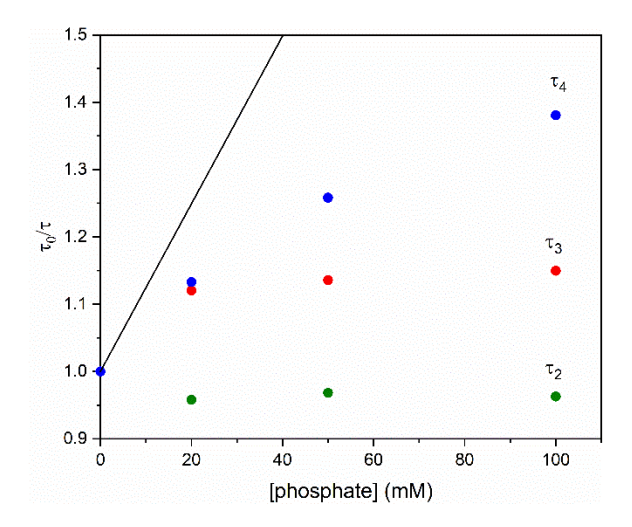


Figure 4. Effect of phosphate concentration on the lifetime components measured for 2AP incorporated into duplex DNA at pH 7.  $\tau_0$  refers to the fluorescence lifetime measured in the absence of phosphate.  $\tau_2$ - $\tau_4$  represent the three longer lifetimes obtained in the fit. The shorter lifetime,  $\tau_1$ , was not determined with sufficient precision and is not included in this analysis. All data are compiled in Table1. The solid line represents the slope determined for free 2AP in the same buffer (Fig. 2C).

#### 3.5 Identification of the individual tautomers of 2AP in water at pH 5-9

Neely et al. have shown that the apparent single exponential decays of 2AP in water arise from two emitting species with lifetimes that cannot be resolved within the typical signal-to-noise ratio of the measurement.<sup>37</sup> When fitted with a single exponential term, the recovered lifetime was found to increase with increasing excitation and emission wavelength.<sup>37</sup> Global fitting using two exponential terms revealed the existence of two species that were attributed to the two most stable tautomeric forms of 2AP (9H 2AP and 7H 2AP, see Fig. 1). Comparison with data measured with 2APr, in which the 7H tautomer is precluded, allowed the authors to assign the species with the longer lifetime and red-shifted spectrum to the less stable 7H tautomer. Based on these observations, it is plausible that our inability to fit the 2AP decays measured in phosphate buffer at pH 9 with a single exponential is due to the lifetimes of the two tautomers becoming noticeably different due to quenching. To investigate this possibility further, we measured fluorescence intensity decays at pH 5 and 9, spanning various emission wavelengths and varying phosphate concentrations.

The contributions of the 7H and 9H tautomers of 2AP to the measured fluorescence intensity decay were determined by analyzing seven intensity decays ( $\lambda_{\text{exc}} = 310 \text{ nm}$ ,  $\lambda_{\text{em}} = 350 - 410 \text{ nm}$ ) simultaneously assuming wavelength-independent lifetimes and wavelength-dependent amplitudes as described by Neely et al.<sup>37</sup> (see materials and methods). All fitting parameters are compiled in Tables 2-4. In pure water, the fitted lifetimes were 10.6 ns and 13.2 ns (Table 2). The wavelength-dependent fractional contribution of each lifetime  $(\tau_{1,2})$  to the steady-state intensity was calculated as  $f_i = \alpha_i \tau_i / (\alpha_1 \tau_1 + \alpha_2 \tau_2)$ , where i=1,2 and  $(\alpha_1+\alpha_2)=1$ . Results are shown in Fig. 5B, where each point represents  $F_{1,2}=f_{1,2}\times F_{ss}$ and  $F_{ss}$  is the steady-state intensity at each wavelength. These findings align closely with the lifetimes and spectra reported by Neely et al.<sup>37</sup> In line with this previous study, we observed that the spectrum of the longest lifetime is red-shifted with respect to the spectrum of the species with the shortest lifetime. The shortest lifetime (10.6 ns in our study) is in good agreement with the lifetime of 2APr measured under identical conditions (10.4 ns), and is therefore likely to arise from emission of the 9H tautomer as suggested previously.<sup>37</sup> The analysis of the data acquired at pH 9 in the absence of phosphates (i.e. dilute NaOH) yielded comparable findings. A global analysis of the seven measured decays using two exponential terms provided a satisfactory description of the data (see Table 2 and Fig. 5C). The fitted lifetimes were determined to be 10.6 ns and 13.8 ns, and the computed spectra closely resembled those obtained at pH 7. The global fit at pH 5 in the absence of phosphate (i.e. dilute HCl) yielded  $\tau_1$  =10. 8 ns and  $\tau_2$  =12. 7 ns and the spectra shown in Fig. Fig 5A. The difference with the spectra obtained at pH 9 is relatively small, particularly when considering the inherent uncertainties associated with the fitted amplitudes when dealing with two lifetimes of similar magnitude. Therefore, although it is possible that the tautomeric population and the individual lifetimes may exhibit a small dependence on pH within this range, these data alone do not provide sufficient evidence for a definitive conclusion.

Table 2. 2AP in HCl (pH = 5), pure water (pH = 7) and NaOH (pH = 9). Results of Global Fitting of all decay curves to a biexponential function with wavelength-independent lifetimes ( $\tau_1$ ,  $\tau_2$ ) and wavelength-dependent amplitudes ( $A_1$ ,  $A_2$ ).

	pH 5		рŀ	17	pH 9		
	$\tau_1$ = 10.8 ns	$\tau_2$ = 12.7 ns	$\tau_1$ = 10.6 ns	$\tau_2$ = 13.2 ns	$\tau_1$ = 10.6 ns	$\tau_2$ = 13.8 ns	
λ <sub>em</sub> (nm)	<b>A</b> <sub>1</sub>	A <sub>2</sub>	<b>A</b> <sub>1</sub>	A <sub>2</sub>	<b>A</b> 1	A <sub>2</sub>	
350	0.65	0.35	0.68	0.32	0.70	0.30	
360	0.57	0.43	0.63	0.37	0.66	0.34	
370	0.52	0.48	0.59	0.41	0.64	0.36	
380	0.48	0.52	0.56	0.44	0.63	0.37	
390	0.43	0.57	0.53	0.47	0.58	0.42	
400	0.42	0.58	0.51	0.49	0.56	0.44	
410	0.40	0.60	0.49	0.51	0.55	0.45	

# 3.6 Effect of $H_2PO_4^-$ and $HPO_4^{2-}$ on the fluorescence of the individual tautomers of 2AP

The measurements described above were repeated at various phosphate concentrations at both pH 5 and pH 9. At pH 9, all intensity decays were adequately fitted with two exponential terms (see Table 3, and Fig. S5 for examples of fitted curves and residuals). The Stern-Volmer analysis of the two lifetimes recovered in each global fit (Fig. 5D) unveiled that the  $HPO_4^{2-}$  anion exhibits a higher quenching efficiency toward the shorter lifetime ( $\tau_1$  =10.6 ns in the absence of phosphate) compared to the longer one ( $\tau_2$  =13.8 ns). The bimolecular quenching constants calculated from the slopes of the plots in Fig. 5D are  $k_{q,1}$  = 1.2 × 10<sup>9</sup> M<sup>-1</sup>.s<sup>-1</sup> and  $k_{q,2}$  = 4.4 × 10<sup>8</sup> M<sup>-1</sup>.s<sup>-1</sup> (for  $\tau_1$  and  $\tau_2$ , respectively). Remarkably, the Stern-Volmer plot of  $\tau_1$  exhibited a substantial overlap with the plot calculated from the lifetimes measured using 2APr under the same conditions (Table S4 and Fig. 5D).

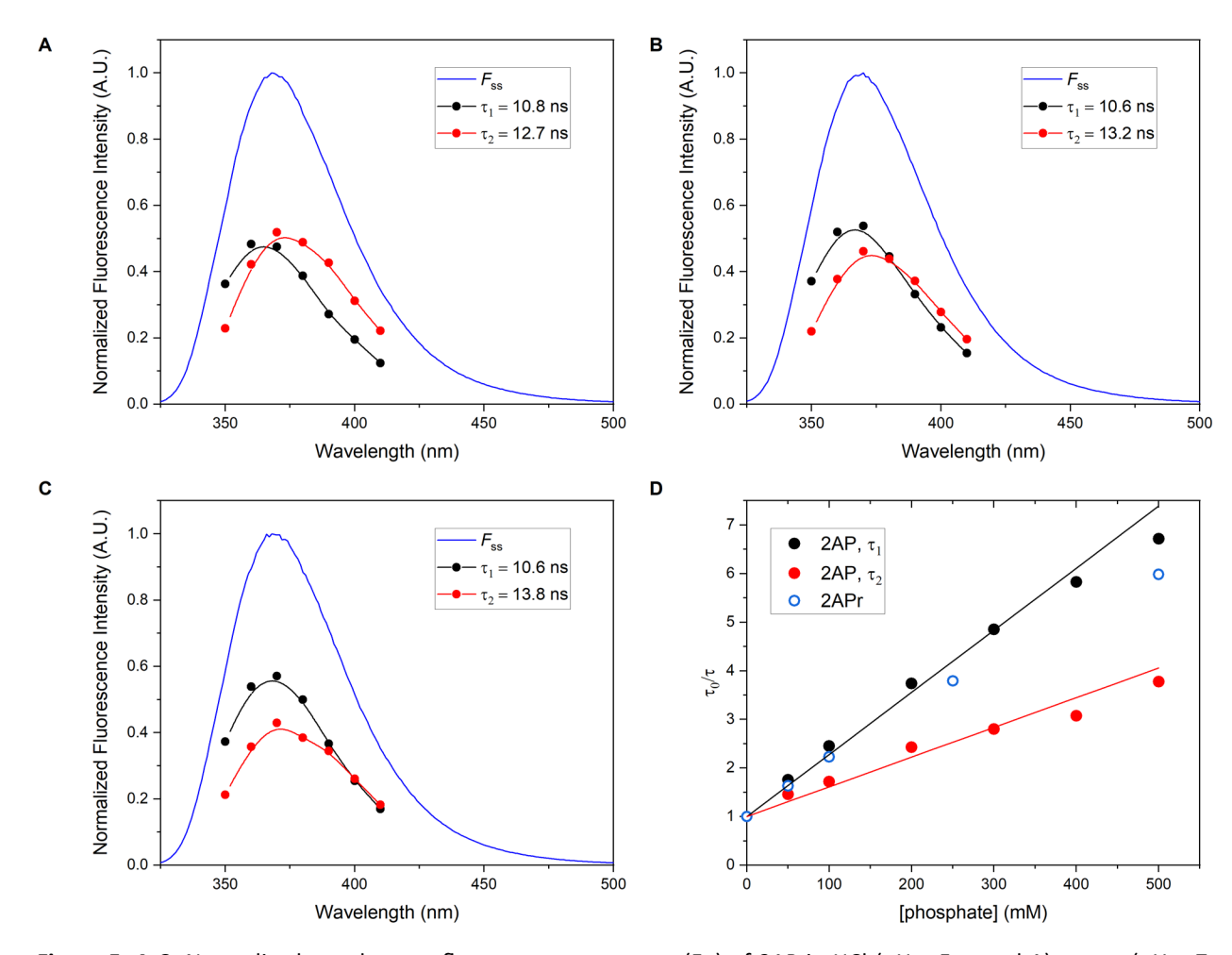


Figure 5. A-C: Normalized steady state fluorescence spectrum ( $F_{ss}$ ) of 2AP in HCl (pH = 5, panel A), water (pH = 7, panel B), and NaOH (pH = 9, panel C). The black and red circles represent the contribution of each lifetime ( $\tau_{1,2}$ ) to the steady-state intensity, calculated as  $F_{ss} \times \alpha_{1,2} \tau_{1,2}/(\alpha_1 \tau_1 + \alpha_2 \tau_2)$ . **D:** Effect of phosphate (pH 9) on the lifetime of 2APr (hollow blue circles), and the two lifetimes determined for 2AP (solid black and solid red circles).  $\tau_0$  refers to the fluorescence lifetime measured in the absence of phosphate.

Table 3. Results of Global Fitting for 2AP in phosphate buffer (pH 9) as a function of phosphate concentration. All decay curves were fit to a biexponential function with wavelength-independent lifetimes ( $\tau_1$ ,  $\tau_2$ ) and wavelength-dependent amplitudes:  $I(\lambda_{em},t) = A_1(\lambda_{em})e^{-t/\tau_1} + A_2(\lambda_{em})e^{-t/\tau_2}$ ,  $\alpha_{1,2} = A_{1,2}/(A_1 + A_2)$ 

	0 mM <sup>(a)</sup> 50 mM		100 mM	200 mM	300 mM	400 mM	500 mM
	$\tau_1 = 10.6 \text{ ns}$	$\tau_1 = 6.1 \text{ ns}$	$\tau_1 = 4.3 \text{ ns}$	$\tau_1 = 2.8 \text{ ns}$	$\tau_1 = 2.1 \text{ ns}$	$\tau_1 = 1.8 \text{ ns}$	$\tau_1 = 1.5 \text{ ns}$
	$\tau_2$ = 13.8 ns	$\tau_2 = 9.5 \text{ ns}$	$\tau_2 = 8.1 \text{ ns}$	$\tau_2 = 5.7 \text{ ns}$	$\tau_2 = 4.9 \text{ ns}$	$\tau_2 = 4.5 \text{ ns}$	$\tau_2 = 3.2 \text{ ns}$
λ <sub>em</sub> (nm)				${lpha_1}^{ ext{(b)}}$			
350	0.70	0.85	0.91	0.91	0.92	0.94	0.86
360	0.66	0.82	0.90	0.89	0.92	0.93	0.85
370	0.64	0.80	0.90	0.89	0.92	0.93	0.85
380	0.63	0.79	0.90	0.88	0.92	0.93	0.85
390	0.58	0.77	0.89	0.87	0.91	0.92	0.85
400	0.56	0.75	0.89	0.87	0.91	0.92	0.85
410	0.55	0.74	0.89	0.87	0.91	0.93	0.86

<sup>(</sup>a) 2AP in NaOH at pH 9 (Table 2). (b)  $\alpha_2=1-\alpha_1$ 

The fluorescence intensity decay arising from a mixture of two non-interacting species is anticipated to exhibit bi-exponential behavior with relative amplitudes  $(\alpha_1/\alpha_2)$  determined by the relative concentrations of each  $(C_1/C_2)$  as well as their relative extinction coefficients at the excitation wavelength  $(\varepsilon_1(\lambda_{exc})/\varepsilon_2(\lambda_{exc}))$ , relative radiative decay rates  $(\Gamma_1/\Gamma_2)$ , and relative values of their spectral emission contours (spectral shapes) measured at the emission wavelength  $(F_1(\lambda_{em})/F_2(\lambda_{em}))$ :

$$\frac{\alpha_1}{\alpha_2}(\lambda_{exc}, \lambda_{em}) = \frac{\varepsilon_{1(\lambda_{exc})}}{\varepsilon_2(\lambda_{exc})} \frac{C_1}{C_2} \frac{\Gamma_1}{\Gamma_2} \frac{F_1(\lambda_{em})}{F_2(\lambda_{em})}$$
(Eq. 1)

The wavelength-dependent pre-exponential factors determined in the absence of phosphate (Table 2) are consistent with a shorter-lived tautomer ( $\tau_1$ ) that exhibits a blue-shifted spectrum with respect to the longer-lived tautomer ( $\tau_2$ ). That is, the decrease in  $\alpha_1/\alpha_2$  observed at increasing  $\lambda_{em}$  values reflects the decrease in  $F_1(\lambda_{em})/F_2(\lambda_{em})$  observed in Fig. 5B. Collisional quenching, however, is not expected to result in changes in the pre-exponential factors (as per Eq. 1). Yet, as shown in Table 3, the addition of phosphate resulted in significant changes in  $\alpha_1$  and  $\alpha_2$ .

Experiments at pH 5 and  $[H_2PO_4^-]=50~mM$  could be fitted with two lifetimes:  $\tau_1=8.0$  and  $\tau_2=6.5$ . The value of  $\tau_1$  coincided with the lifetime determined for 2APr under the same conditions (Table S4) and is therefore likely to represent emission from the 9H tautomer. In contrast to the data acquired at pH 9, at pH 5  $\tau_0/\tau$  was greater for  $\tau_2$  than for  $\tau_1$ , suggesting that the 7H tautomer of 2AP is more efficiently quenched by the ion  $H_2PO_4^-$  than the 9H. However, as the concentration of phosphate increased beyond this point, neither fitted lifetime resembled the lifetime measured with 2APr under the same conditions (see **tables 4 and S4**). Constructing Stern-Volmer plots akin Fig. 5D posed a challenge because, unlike pH 9, we were unable to use the 2APr data to assign a particular lifetime to a particular tautomer. Moreover, at pH 9, the higher quenching constant was associated with the shortest lifetime and this resulted in lifetimes that became increasingly different with increasing phosphate concentration. In contrast, at pH 5,

the longest lifetime was quenched more efficiently, resulting in lifetimes of similar magnitude that could not be definitely assigned to either tautomer. Additionally, fitting fluorescence decays with two exponentials is challenging when the two lifetimes are close because this can lead to parameter correlation and diminish the ability to differentiate between the two decay components.

Table 4. Results of Global Fitting for 2AP in phosphate buffer (pH 5) as a function of phosphate concentration. All decay curves were fit to a biexponential function with wavelength-independent lifetimes ( $\tau_1$ ,  $\tau_2$ ) and wavelength-dependent amplitudes:  $I(\lambda_{em},t) = A_1(\lambda_{em})e^{-t/\tau_1} + A_2(\lambda_{em})e^{-t/\tau_2}$ ,  $\alpha_{1,2} = A_{1,2}/(A_1 + A_2)$ 

	0 mM <sup>(a)</sup>	50 mM	100 mM	250 mM	500 mM			
	$\tau_1$ = 10.8 ns	$\tau_1 = 8.0 \text{ ns}$	$\tau_1 = 5.1 \text{ ns}$	$\tau_1 = 3.3 \text{ ns}$	$\tau_1 = 2.2 \text{ ns}$			
	$\tau_2 = 12.7 \text{ ns}$	$\tau_2 = 6.5 \text{ ns}$	$\tau_2 = 5.9 \text{ ns}$	$\tau_2 = 3.0 \text{ ns}$	$\tau_2 = 1.6 \text{ ns}$			
λ <sub>em</sub> (nm)			$\alpha_1^{(b)}$	α <sub>1</sub> (b)				
350	0.65	0.54	0.69	0.38	0.56			
360	0.57	0.64	0.58	0.54	0.67			
370	0.52	0.70	0.49	0.67	0.74			
380	0.48	0.71	0.41	0.82	0.80			
390	0.43	0.77	0.35	0.95	0.86			
400	0.42	0.81	0.28	1.08 <sup>(c)</sup>	0.89			
410	0.40	0.85	0.23	1.17 <sup>(c)</sup>	0.93			

(a)2AP in HCl at pH 5 (Table 2). (b)  $\alpha_2=1-\alpha_1$ , (c)  $\alpha_2$  < 0

#### **4 DISCUSSION**

The fluorescence intensity decay arising from a mixture of two species is anticipated to exhibit biexponential behavior with relative amplitudes determined by the relative concentrations of each, as well as their spectral and photophysical properties (Eq. 1). The addition of phosphate to 2AP does not result in significant spectral changes (Fig S2), and significant changes to the extinction coefficients and radiative constants are not anticipated. Therefore, for two non-interacting fluorescent species that are quenched independently by a collisional mechanism, lifetimes are expected to decrease according to the Stern-Volmer equation without changes in  $\alpha_1/\alpha_2$ . As shown in Table 3, however, the addition of phosphate at pH 9 resulted in a significant increase in  $\alpha_1$ . As previously mentioned, the added complexity of the data collected at pH 5 rendered the analysis of preexponential factors unfeasible. The changes in  $\alpha_1/\alpha_2$ observed at pH 9 may indicate a change in the relative populations of the two emitting tautomers ( $C_1/C_2$ , see Eq. 1) at increasing concentrations of phosphate. In support of this, theoretical and experimental solidstate studies have concluded that non-covalent interactions can influence the equilibrium between tautomeric forms of adenine. For instance, a number of crystallographic structures of complexes containing adenine show a metal ion coordinated to the N9 atom, causing the hydrogen to shift to the N7 position. The resulting tautomer may be further stabilized by H-bonding interactions with water or other ligands.<sup>38-40</sup> Computational studies also suggest tautomeric population shifts resulting from cooperative effects between metal ions and H-bond acceptors. For instance, binding of Mg<sup>2+</sup>, Cu<sup>2+</sup>, or Zn<sup>2+</sup> to adenine in the presence of ammonia was predicted to induce the transfer of an adenine NH<sub>2</sub> proton to ammonia, resulting in the stabilization of an imino tautomer over the canonical amino form. <sup>41</sup> Another computational study reported that interactions between adenine, Na<sup>+</sup> and acetate ions (but not acetic acid) stabilize the 7H-amino, 1H-amino, and 3H-9H imino tautomers over the canonical 9H-amino form.<sup>42</sup> In this case,

calculated energies suggest that these rare tautomers of adenine would coexist with the 9H tautomer when complexed with acetate and Na<sup>+</sup> ions.

However, a tautomeric shift caused by non-covalent interactions between ground state 2AP and the phosphate ions does not explain the quenching trends observed experimentally. Ground state interactions that lead to quenching would result in a significant static component that would cause large differences in the slopes of the intensity- and lifetime-based plots of Figs. 2C.<sup>43</sup> Simultaneous quenching by complex formation and collisions would give rise to a characteristic upward curvature in the intensity-based plot that we did not observe. The fact that our data is consistent with a predominantly dynamic mechanism indicates that the interactions between 2AP and the phosphate ions that are responsible for quenching occur in the excited state. As stated above, a collisional mechanism where the fluorophore is assumed to be quenched instantaneously upon collision with the quencher is not expected to cause the changes in pre-exponential factors observed experimentally. To explore the potential role of transient interactions in the excited state as a plausible explanation for the data we have observed, we examined the kinetic scheme depicted in Fig. 6. In this model, "A" refers to free 2AP, while "B" represents a non-covalent complex formed between 2AP and either  $H_2PO_4^-$  or  $HPO_4^{2-}$  (denoted by P). The values of  $k_A$  and  $k_B$  are related to the radiative decay rates ( $\Gamma_B$ ,  $\Gamma_A$ ), through the corresponding fluorescence quantum yields:  $\Gamma_A = \phi_A k_A$ ,  $\Gamma_B = \phi_B k_B$ .

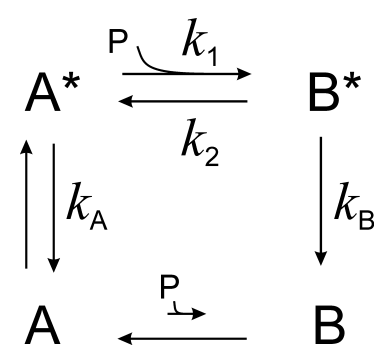


**Figure 6.** Kinetic scheme showing the formation of a non-covalent complex (B) between 2AP (A) and either  $H_2PO_4^-$  or  $HPO_4^{2-}$  (P). The reaction is assumed to be negligible in the ground state.  $k_{A,B} = \Gamma_{A,B}/\phi_{A,B}$ , where Γ represents the radiative decay rate and  $\phi$  is the fluorescence quantum yield.

The differential equations for the decay of the excited states of free 2AP (A\*) and 2AP complexed with phosphate (B\*) are given in the Supporting Information file (Eq. S1). Integration of these equations with  $[A^*] = [A^*]_0$  and  $[B^*] = 0$  at t = 0 yields the expressions for  $[A^*](t)$  and  $[B^*](t)$  given in Eqs. S2 and S3. The fluorescence decays of A and B at wavelength  $\lambda_{em}$  depend on the concentrations of the corresponding excited states,  $[A^*](t)$  and  $[B^*](t)$ , the radiative decay rates  $(\Gamma_B, \Gamma_A)$ , and the values of the spectral emission contours (spectral shapes) at the emission wavelength,  $F_A(\lambda_{em})$  and  $F_B(\lambda_{em})$  (Eqs. S11-S12). The resulting mathematical expressions for the time-dependent and wavelength-dependent fluorescence intensity decays of A and B are:

$$I_A(\lambda_{em},t) = \alpha_1(\lambda_{em})e^{-t/\tau_1} + \alpha_2(\lambda_{em})e^{-t/\tau_2}$$
 Eq. 2

$$I_B(\lambda_{em}, t) = \beta_1(\lambda_{em})e^{-t/\tau_1} + \beta_2(\lambda_{em})e^{-t/\tau_2}$$
 Eq. 3

where

$$\tau_1 = 2(X + Y + W)^{-1}$$
 Eq. 4

$$\tau_2 = 2(X + Y - W)^{-1}$$
 Eq. 5

$$\alpha_1(\lambda_{em}) = \frac{[A^*]_0 \Gamma_{\!\!A}.F_{\!\!A}(\lambda_{em})}{\tau_1^{-1} - \tau_2^{-1}} (X - \tau_2^{-1}) \label{eq:alpha_em}$$
 Eq. 6

$$\alpha_2(\lambda_{em}) \frac{[A^*]_0 \Gamma_A F_A(\lambda_{em})}{\tau_1^{-1} - \tau_2^{-1}} (\tau_1^{-1} - X)$$
 Eq. 7

$$\beta_1(\lambda_{em}) = -\frac{[A^*]_0 \Gamma_B F_B(\lambda_{em})}{\tau_1^{-1} - \tau_2^{-1}} k_1[P]$$
 Eq. 8

$$\beta_2(\lambda_{em}) = \frac{[A^*]_0 \Gamma_B F_B(\lambda_{em})}{\tau_1^{-1} - \tau_2^{-1}} k_1[P]$$
 Eq. 9

and 
$$X = k_A + k_1[P]$$
,  $Y = k_B + k_2$ , and  $W = [4k_2k_1[P] + (Y - X)^2]^{1/2}$  (Eqs. S6-S8).

The total emission arising from each tautomer can be then expressed as  $I_A(\lambda_{em}, t) + I_B(\lambda_{em}, t)$ :

$$I_{T}(\lambda_{em}, t) = \frac{[A^{*}]_{0}}{\tau_{1}^{-1} - \tau_{2}^{-1}} \Big[ [(X - \tau_{2}^{-1})\Gamma_{A}.F_{A}(\lambda_{em}) - k_{1}[P]\Gamma_{B}.F_{B}(\lambda_{em})]e^{-t/\tau_{1}} + [(\tau_{1}^{-1} - X)\Gamma_{A}.F_{A}(\lambda_{em}) + k_{1}[P]\Gamma_{B}.F_{B}(\lambda_{em})]e^{-t/\tau_{2}} \Big]$$
Eq. 10

Inspection of these equations shows that, in contrast to a simple dynamic quenching process,  $I_A(\lambda_{em}, t)$ is predicted to be bi-exponential even if B is non-fluorescent. That is, according to the mechanism of Fig. 6, the fluorescence intensity decays of each individual 2AP tautomer are no longer expected to be monoexponential in the presence of phosphate. The two lifetimes,  $\tau_1$  and  $\tau_2$ , are the same for the decay of both species (A and B) and depend on all rate constants defined on Fig. 6 as well as on phosphate concentration. The fact that all 2APr decays were observed to be monoexponential at all measured phosphate concentrations may appear to be inconsistent with this model. However, inspection of Eqs. 2-9 shows that only one of the two lifetimes is anticipated to show a significant dependance on quencher concentration when  $k_2 \ll k_1[P].$  This condition, and the fact that the magnitude of  $k_1[P]$  should be comparable or greater than  $\emph{k}_\emph{A}$  for quenching to be significant, lead to simplified expressions for the two lifetimes:  $\tau_1^{-1} \approx k_B$ , and  $\tau_2^{-1} \approx k_A + k_1[P]$ . Additionally, if these conditions are met, the pre-exponential factor for  $au_1$  is predicted to be orders of magnitude smaller than the pre-exponential factor for  $au_2$  (which depends on [P]) when  $\phi_B << \phi_A$ . Examples of Stern-Volmer plots and pre-exponential amplitudes expected for a single species "A" (e.g. 2APr) that interacts with a quencher (e.g. phosphate) in the excited state according to the mechanism of Fig. 6 are shown in the Supporting Information file (Fig. S6). Case I assumes a combination of parameters consistent with the conditions described above, which predict a decay that can be approximated by a single exponential with a lifetime that depends on phosphate concentration as described by the Stern-Volmer equation. Case II shows that a bi-exponential decay with a non-negligible negative amplitude is expected for one of the lifetimes at increasing values of  $\phi_B$ . Additionally, as shown in case III, it is still possible to observe monoexponential fluorescence decay kinetics and a linear Stern-Volmer plot for values of  $k_2$  that are comparable to or greater than  $k_1[P]$ . In this case, however, the extracted Stern-Volmer constant is lower than the value expected for a simple dynamic mechanism ( $K_{SV}=k_1k_A^{-1}$ ). The results of this analysis indicate that the monoexponential intensity decays measured with 2APr are consistent with the mechanism of Fig. 6 for certain combinations of rate constants and photophysical parameters. However, as in Case III (Fig. S6), the slope of the Stern-Volmer plot may be lower than the value predicted for a simple dynamic mechanism and this may lead to an underestimated value of the bimolecular quenching constant,  $k_1$ .

For 2AP, the two lifetimes recovered experimentally depend strongly on phosphate concentration (Tables 3 and 4). While one of the lifetimes determined at pH 9 resembled the lifetime measured with 2APr under the same conditions, this was not the case at pH 5. While for free 2AP (no quencher) one expects one of the measured lifetimes to resemble the lifetime of the riboside, this is not necessarily the case for the mechanism presented in Fig. 6 when quencher is present. The interactions between phosphate ions and 2APr or 9H 2AP, which determine k<sub>1</sub> and k<sub>2</sub>, might differ because of the additional hydrogen atom in 2AP that can serve as an H-bond donor. To rationalize the results obtained with 2AP (Figure 5D) we considered the total fluorescence intensity expected for two tautomers that co-exist in the ground state and are quenched independently by the mechanism of Fig. 6. In this case, the total fluorescence intensity can be calculated as the sum of two bi-exponential decays, each described by Eq. 10 with parameters that may differ for each tautomer. In particular, the relative values of  $F_A(\lambda_{em})$  for each tautomer depend on emission wavelength due to the spectral differences discussed previously. Our results also suggest that the interactions between the phosphate ions and the excited state of 2AP are different for the two tautomers. Attempting to extract the four lifetimes expected for this model from our experiments is unrealistic given the significant spectral overlap and similar lifetimes of the two tautomers. Instead, to assess whether this model provides a plausible explanation for our data, we calculated predicted  $I_T(\lambda_{em},t)$  decays and fitted the resulting curve with a bi-exponential function, mirroring the analysis performed on the experimental data. This procedure results in two apparent lifetimes and two apparent relative amplitudes that can be contrasted with the fitting parameters obtained from fitting experimental data. Fig. 7 summarizes the results of this analysis. We considered two species (denoted 1 and 2, presumed to be the 9H and 7H tautomers) with  $k_A$  values consistent with the lifetimes measured for the individual tautomers at pH 9 in the absence of quenchers:  $k_{A1}=10^8 s^{-1}$  and  $k_{A2}=0.8\times 10^8 s^{-1}$  . Values for  $k_1$  were assumed to be  $k_{11} = 0.5 \times 10^9 M^{-1} s^{-1}$  (for species 1) and  $k_{12} = 1.5 \times 10^9 M^{-1} s^{-1}$  (species 2). Values of the order of  $10^9 M^{-1} s^{-1}$  were required for quenching to be efficient at the concentrations of quencher used in this study, and a difference of at least 2-fold was needed for the two resulting lifetimes to show a difference in the quenching constants similar to that observed experimentally (Fig. 5D). The values of  $\,k_2$  were assumed to be the same for both tautomers for simplicity and equal to  $k_2 = 1 \times 10^5 s^{-1}$ . The value of  $k_2$  has only a small effect in the lifetimes obtained in the simulations for values lower than approximately  $10^6 s^{-1}$ . The initial concentration of excited-state 2AP ( $[A^*]_0$ ) was assumed to be four times greater for species 1 than for species 2 to account for the different initial concentrations expected for the two tautomers. All other parameters used to generate Fig. 7 are listed in the corresponding figure caption.

As discussed above, each of the tautomers is anticipated to decay with bi-exponential kinetics (Eq. 10), but in each case, only one of the lifetimes may exhibit a significant dependance on quencher concentration. Fig. 7A shows the predicted Stern-Volmer plots for the two expected lifetimes for each tautomer. In this figure,  $\tau_{ij}$  refers to the i-th lifetime for species j. Due to spectral overlap, the total emission expected for a

mixture of species 1 and 2 is predicted to decay with complex kinetics. We mirrored the procedure used experimentally and fitted the calculated emission decays with a bi-exponential function to obtain two apparent lifetimes  $(\tau_1^{app}, \tau_2^{app})$  and their corresponding pre-exponential factors (A<sub>1</sub>, A<sub>2</sub>). We note that these parameters can no longer be linked to a specific tautomer, so the subscripts 1,2 have become arbitrary and do not denote a well-defined species. The apparent lifetimes are shown in Figs 7B and 7C for two different situations that differ in the relative values of  $F_A(\lambda_{em})$  and  $F_B(\lambda_{em})$  for tautomers 1 and 2. For the unbound tautomers (species A),  $F_A(\lambda_{em})$  depends on emission wavelength as the emission of the 7H tautomer is slightly red shifted compared to the 9H tautomer. A value of  $F_{A2}(\lambda_{em})/F_{A1}(\lambda_{em}) = 1.2$  was arbitrarily assumed in all calculations, but we note that the conclusions drawn here do not depend on this assumed value. Figures 7B and 7C differ in the assumed values of  $F_B(\lambda_{em})/F_A(\lambda_{em})$ . For Fig. 7B,  $F_B(\lambda_{em})/F_A(\lambda_{em})$  was assumed to be zero for both tautomers, while this value was set to 0.5 for Fig. 7C. Increasing values of  $F_B(\lambda_{em})/F_A(\lambda_{em})$  indicate increasing contributions of species B (bound 2AP) to the measured fluorescence.

In both cases (Figs. 7B and 7C), the two fitted apparent lifetimes are expected to depend on quencher concentration, but we note that the slopes of these plots depend on the spectral characteristics of all species involved and do not directly reflect the values of the bimolecular quenching constants ( $k_1$ ) as would be the case for a simple dynamic quenching mechanism. Additionally, results show that a downward curvature in the Stern-Volmer plot can be expected when  $F_B(\lambda_{em})/F_A(\lambda_{em}) \neq 0$  (Fig. 7C). As discussed above, we were initially hesitant to interpret the downward curvatures observed in our experiments with phosphate (Fig. 2C) due to a series of reports that suggest that the ions  $H_2PO_4^-$  and  $HPO_4^2^-$  may self-associate at elevated concentrations. <sup>21-24</sup> However, we now note that this model predicts such a curvature, suggesting that the observed curvature observed in Figs. 2C and 5D may be a consequence of transient interactions between the phosphate ions and the excited states of the two tautomers of 2AP.

Another major result of the analysis presented above is that, for this model, the fitted preexponential factors are predicted to depend on quencher concentration. As shown in Fig. 7D, for the two cases considered in Figs. 7B and 7C, the value of  $A_1$  is predicted to increase steeply at moderate phosphate concentrations. Furthermore, for the conditions used in Fig. 7C,  $A_1$  is predicted to decrease slowly at higher values, in line with our experimental observations (Table 3, [Phosphate] > 400 mM). Overall, although it is impossible to claim that all parameters used in this analysis are good estimates of the kinetic constants for all processes involved, we have shown that transient interactions between the individual tautomers and the phosphate ions, modeled with the mechanism of Fig. 6, provide a plausible explanation for the experimental observations.

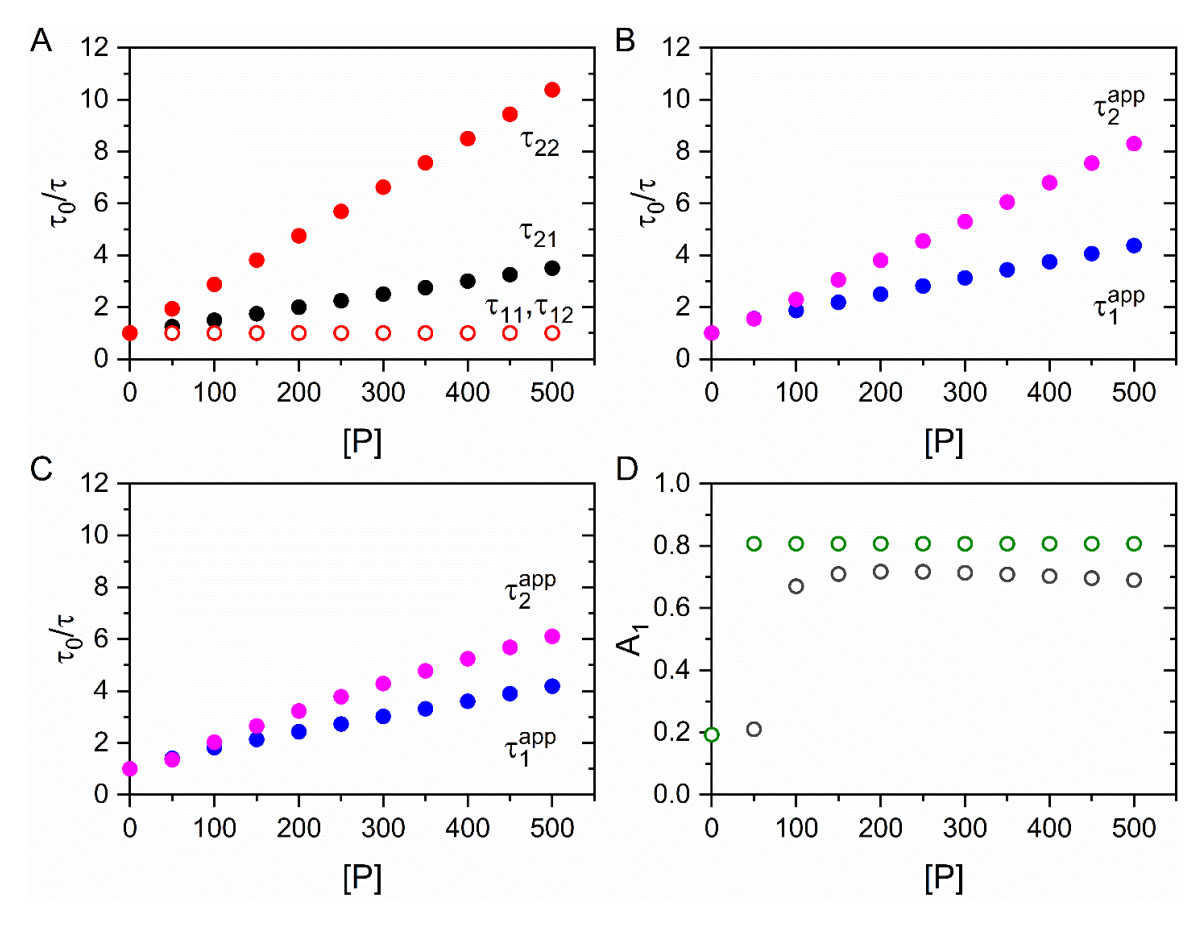


Figure 7. A) Predicted Stern-Volmer plots for the two expected lifetimes for each tautomer.  $\tau_{ij}$  refers to the i-th lifetime for species j. Parameters used in the calculation were:  $k_{A1}=10^8s^{-1}$  (species 1),  $k_{A2}=0.8\times10^8s^{-1}$  (species 2),  $k_{21}=k_{22}=1\times10^5s^{-1}$ ,  $\frac{[A^*]_{01}}{[A^*]_{02}}=4$ ,  $\Gamma_{B1}=\Gamma_{B2}=1\times10^{10}s^{-1}$ ,  $\varphi_{B1}=\varphi_{B2}=0.01$ . Black symbols correspond to species 1 and red symbols correspond to species 2. The hollow symbols ( $\tau_1$  for species 1 and 2) overlap. B) Predicted Stern-Volmer plots for the two expected apparent lifetimes obtained when fitting the complex decay expected for a mixture of species 1 and 2 with a bi-exponential function. Additional parameters used in this calculation were:  $F_{A2}(\lambda_{em})/F_{A1}(\lambda_{em})=1.2$ ,  $\frac{F_B(\lambda_{em})}{F_A(\lambda_{em})}=0$  for both species. C) same as B) but with  $\frac{F_B(\lambda_{em})}{F_A(\lambda_{em})}=0.5$ . D) Pre-exponential factor for  $\tau_1^{app}$ . Green circles: conditions of panel B), Grey circles: conditions of panel C). Both overlap at [P] = 0.

Previous studies have demonstrated that proton donors can quench indole fluorescence through an excited-state proton transfer mechanism. These proton transfer reactions are characterized by deuterium isotope effects. To investigate this possibility, quenching experiments were repeated by replacing  $H_2PO_4^-$  and water by  $D_2PO_4^-$  and  $D_2O$ . As shown in Fig. S7, using deuterated compounds had a negligible effect on the measured fluorescence lifetime and fluorescence quantum yield of 2AP. Instead, we propose that 2AP quenching by phosphate ions is due to the formation of a non-covalent complex similar to the ones predicted in a gas-phase computational study of adenine complexed with acetate and sodium ions (Fig. S8). In this study, the authors determined that coordination of the ions  $Na^+$  and  $CH_3COO^-$  stabilize the adenine tautomers to different extents, resulting in the preferential stabilization of the 7H and 1H amino-tautomers over the otherwise more stable 9H tautomer. This is not surprising considering

that these geometries allow the formation of two H-bonds that involve a hydrogen from the adenine amino group and the hydrogen bound to either N7 or N1. Instead, the complex with the 9H tautomer involves hydrogen bonds with a less favorable geometry. In the most stable structure (7H-adenine), the sodium atom is coordinated with N3 and N9, while the acetate ion coordinates through two H-bonds (Fig. S8). The first is between a negatively charged oxygen atom of the acetate ion and an amino proton (NH<sub>2</sub>) of adenine, and the second is between another oxygen atom of acetate and the 7H hydrogen of 7H-adenine. Interestingly, these calculations show that the 7H proton is transferred from the adenine base to the acetate ion, which would explain loss of fluorescence (quenching of 2AP was observed in water at high pH values, Table S1). We note that a previous publication by the same group, published in Ukrainian, reported the results of a study of the interactions between 2AP and the acetate ion. <sup>45</sup> These calculations were performed with a lower level of theory compared to the 2004 publication (ref. 42), so predicted relative energies may not be as accurate. Additionally, the contribution of the cation, which was found to be considerable in ref. <sup>42</sup>, was not taken into consideration. Despite these limitations, it is intersting to note that this study predicts that the coordination of 2AP with acetate ions results in the stabilization of the 3H tautomer of 2AP over the rest due to a more favorable geometry for efficient H-bonding.

Our experimental results are insufficient to determine the exact nature of the 2AP-phosphate interactions that lead to quenching of 2AP in the excited state, and we cannot rule out the possibility that these interactions change the tautomeric composition of 2AP as predicted in gas-phase quantum mechanical calculations. Yet, the fact that we observed quenching by the phosphate and carbonate ions, but not sulphate, supports the proposal that the quencher acts as a H-bond acceptor. Reports of fluorescence quenching by MOPS and HEPES are limited. However, we note that MOPS was found to be an efficient electron donor<sup>46</sup> and may therefore quench 2AP by photoinduced electron transfer. Further research would be needed to ellucidate whether PET is responsible for quenching of 2AP by MOPS and HEPES, or whether all anions used in this study share a common quenching mechanism.

#### **5 CONCLUSIONS**

Our results show that the fluorescence of 2AP is significantly quenched in phosphate, MOPS, HEPES and carbonate buffers. While phosphate ions have been documented to quench the fluorescence of tyrosine, <sup>26</sup>-<sup>28</sup> tryptophan,<sup>29</sup> and other organic molecules,<sup>30-32</sup> these ions are not typically recognized as common quenchers. We were not able to find repots of fluorescence quenching of organic molecules by carbonate or bicarbonate ions, and to our knowledge, quenching by MOPS and HEPS has been reported in only one publication.<sup>25</sup> Quenching markedly affects the fluorescence quantum yield and lifetime of the fluorophore, with important repercussions for interpretating 2AP fluorescence signals when this probe is used as a fluorescent analog of adenine in DNA and RNA research. The results of this study are consistent with a dynamic quenching mechanism in all cases. However, a detailed analysis of the wavelength-dependent fluorescence intensity decays measured in phosphate buffer reveals a more complex scenario that points to transient interactions between the excited state of 2AP and the ion. The differences observed for 2APr, 9H 2AP and 7H 2AP suggest that the interactions between the  $H_2PO_4^-$  and  $HPO_4^{2-}$  ions and each of these species are not identical. Although we cannot determine the precise nature of these interactions, all results, including the fact that the sulphate ion does not quench 2AP fluorescence, suggest that the phosphate ions interact with 2AP in the excited state, acting as H-bond acceptors. Future work will seek to determine if other anions that are conjugate bases of weak organic acids (e.g. acetate) quench 2AP fluorescence by the same mechanism. Our results in carbonate buffer indicate that quenching is efficient,

but performing time-resolved experiments at various emission wavelengths will be essential for identifying the 2AP tautomers and assessing the influence of the carbonate ion on each.

#### **ACKNOWLEDGEMENTS**

M.L. acknowledges use of the Ultrafast Laser Spectroscopy Facility at Arizona State University. This work was supported by the National Science Foundation [# 1918716 to ML].

#### **REFERENCES**

- Jones, A. C. & Neely, R. K. 2-aminopurine as a fluorescent probe of DNA conformation and the DNA-enzyme interface. *Q Rev Biophys* **48**, 244-279 (2015). https://doi.org:10.1017/S0033583514000158
- Wilhelmsson, L. M. Fluorescent nucleic acid base analogues. *Q Rev Biophys* 43, 159-183 (2010). https://doi.org:Doi 10.1017/S0033583510000090
- Anders, A. DNA fluorescence at room temperature excited by means of a dye laser. *Chem Phys Lett* **81**, 270-272 (1981). <a href="https://doi.org/10.1016/0009-2614(81)80250-3">https://doi.org/10.1016/0009-2614(81)80250-3</a>
- 4 Crespo-Hernández, C. E., Cohen, B., Hare, P. M. & Kohler, B. Ultrafast Excited-State Dynamics in Nucleic Acids. *Chem Rev* **104**, 1977-2020 (2004). <a href="https://doi.org:10.1021/cr0206770">https://doi.org:10.1021/cr0206770</a>
- Ward, D. C., Reich, E. & Stryer, L. Fluorescence Studies of Nucleotides and Polynucleotides .I. Formycin 2-Aminopurine Riboside 2,6-Diaminopurine Riboside and Their Derivatives. *J Biol Chem* **244**, 1228-& (1969).
- Avilov, S. V., Piemont, E., Shvadchak, V., de Rocquigny, H. & Mely, Y. Probing dynamics of HIV-1 nucleocapsid protein/target hexanucleotide complexes by 2-aminopurine. *Nucleic Acids Res* **36**, 885-896 (2008). <a href="https://doi.org:10.1093/nar/gkm1109">https://doi.org:10.1093/nar/gkm1109</a>
- Neely, R. K. *et al.* Time-resolved fluorescence of 2-aminopurine as a probe of base flipping in M.Hhal-DNA complexes. *Nucleic Acids Res* **33**, 6953-6960 (2005). https://doi.org:10.1093/nar/gki995
- 8 Guest, C. R., Hochstrasser, R. A., Sowers, L. C. & Millar, D. P. Dynamics of mismatched base pairs in DNA. *Biochemistry* **30**, 3271-3279 (1991). <a href="https://doi.org:10.1021/bi00227a015">https://doi.org:10.1021/bi00227a015</a>
- 9 Rachofsky, E. L., Seibert, E., Stivers, J. T., Osman, R. & Ross, J. B. Conformation and dynamics of abasic sites in DNA investigated by time-resolved fluorescence of 2-aminopurine. *Biochemistry-Us* **40**, 957-967 (2001). <a href="https://doi.org:10.1021/bi001665g">https://doi.org:10.1021/bi001665g</a>
- Allan, B. W. & Reich, N. O. Targeted Base Stacking Disruption by the EcoRI DNA Methyltransferase. *Biochemistry* **35**, 14757-14762 (1996). https://doi.org:10.1021/bi9615708
- Bloom, L. B., Otto, M. R., Beechem, J. M. & Goodman, M. F. Influence of 5'-nearest neighbors on the insertion kinetics of the fluorescent nucleotide analog 2-aminopurine by Klenow fragment. *Biochemistry* **32**, 11247-11258 (1993). https://doi.org:10.1021/bi00092a039
- Lemay, J.-F., Penedo, J. C., Tremblay, R., Lilley, D. M. J. & Lafontaine, Daniel A. Folding of the Adenine Riboswitch. *Chem Biol* **13**, 857-868 (2006). https://doi.org/https://doi.org/10.1016/j.chembiol.2006.06.010
- Serrano-Andrés, L., Merchán, M. & Borin, A. C. Adenine and 2-aminopurine: Paradigms of modern theoretical photochemistry. *P Natl Acad Sci USA* **103**, 8691-8696 (2006). https://doi.org:10.1073/pnas.0602991103
- Dziuba, D. *et al.* Fundamental photophysics of isomorphic and expanded fluorescent nucleoside analogues. *Chem Soc Rev* **50**, 7062-7107 (2021). https://doi.org;10.1039/D1CS00194A
- Lobsiger, S., Blaser, S., Sinha, R. K., Frey, H. M. & Leutwyler, S. Switching on the fluorescence of 2-aminopurine by site-selective microhydration. *Nat Chem* **6**, 989-993 (2014). https://doi.org:10.1038/Nchem.2086

- Paterson, K. A., Arlt, J. & Jones, A. C. Dynamic and static quenching of 2-aminopurine fluorescence by the natural DNA nucleotides in solution. *Methods Appl Fluoresc* **8**, 025002 (2020). https://doi.org:10.1088/2050-6120/ab71c3
- Orndorff, P. B. *et al.* Uracil-DNA glycosylase efficiency is modulated by substrate rigidity. *Sci Rep* **13**, 3915 (2023). https://doi.org:10.1038/s41598-023-30620-0
- Levitus, M. Tutorial: measurement of fluorescence spectra and determination of relative fluorescence quantum yields of transparent samples. *Methods Appl Fluoresc* **8**, 033001 (2020). https://doi.org:10.1088/2050-6120/ab7e10
- 19 Gargallo, R., Vives, M., Tauler, R. & Eritja, R. Protonation studies and multivariate curve resolution on oligodeoxynucleotides carrying the mutagenic base 2-aminopurine. *Biophys J* 81, 2886-2896 (2001). https://doi.org:10.1016/S0006-3495(01)75929-2
- 20 Christensen, J. J., Rytting, J. H. & Izatt, R. M. Thermodynamic pK, ΔH°, ΔS°, and ΔCp° values for proton dissociation from several purines and their nucleosides in aqueous solution. *Biochemistry* **9**, 4907-4913 (1970). <a href="https://doi.org:10.1021/bi00827a012">https://doi.org:10.1021/bi00827a012</a>
- Zhao, W., Flood, A. H. & White, N. G. Recognition and applications of anion-anion dimers based on anti-electrostatic hydrogen bonds (AEHBs). *Chem Soc Rev* **49**, 7893-7906 (2020). https://doi.org:10.1039/d0cs00486c
- Wood, R. H. & Platford, R. F. Free energies of aqueous mixtures of NaH2PO4 and NACIO4: Evidence for the species (H2PO4)2–2. *J Solution Chem* **4**, 977-982 (1975). https://doi.org:10.1007/BF01074739
- Rull, F., Del Valle, A., Sobron, F. & Veintemillas, S. Raman study of phosphate dimerization in aqueous KH2PO4 solutions using a self-deconvolution method. *J Raman Spectrosc* **20**, 625-631 (1989). <a href="https://doi.org/10.1002/jrs.1250200913">https://doi.org/10.1002/jrs.1250200913</a>
- Preston, C. M. & Adams, W. A. A laser Raman spectroscopic study of aqueous orthophosphate salts. *The Journal of Physical Chemistry* **83**, 814-821 (1979). https://doi.org:10.1021/j100470a011
- Werner, T., Fahnrich, K., Huber, C. & Wolfbeis, O. S. Anion-Induced Fluorescence Quenching of a New Zwitterionic Biacridine Derivative. *Photochem Photobiol* **70**, 585-589 (1999). https://doi.org/10.1111/j.1751-1097.1999.tb08255.x
- 26 Chen, R. F. & Cohen, P. F. Quenching of tyrosine fluorescence in proteins by phosphate. *Arch Biochem Biophys* **114**, 514-522 (1966). <a href="https://doi.org:10.1016/0003-9861(66)90375-4">https://doi.org:10.1016/0003-9861(66)90375-4</a>
- Alev-Behmoaras, T., Toulme, J.-J. & Hélène, C. Quenching of Tyrosine Fluorescence by Phosphate Ions: A Model Study for Protein-Nucleic Acid Complexes. *Photochem Photobiol* **30**, 533-539 (1979). <a href="https://doi.org:10.1111/j.1751-1097.1979.tb07177.x">https://doi.org:10.1111/j.1751-1097.1979.tb07177.x</a>
- Shimizu, O., Watanabe, J. & Imakubo, K. Effect of Phosphate Ion on Fluorescent Characteristics of Tyrosine and Its Conjugate Base. *Photochem Photobiol* **29**, 915-919 (1979). https://doi.org;10.1111/j.1751-1097.1979.tb07791.x
- Alev-Behmoaras, T., Toulme, J. J. & Helene, C. Effect of phosphate ions on the fluorescence of tryptophan derivatives. Implications in fluorescence investigation of protein-nucleic acid complexes. *Biochimie* **61**, 957-960 (1979). <a href="https://doi.org:10.1016/s0300-9084(79)80246-1">https://doi.org:10.1016/s0300-9084(79)80246-1</a>
- Cowgill, R. W. Fluorescence and the structure of proteins. I. Effects of substituents on the fluorescence of indole and phenol compounds. *Arch. Biochem. Biophys.* **100**, 36-44 (1963). <a href="https://doi.org/10.1016/0003-9861(63)90031-6">https://doi.org/10.1016/0003-9861(63)90031-6</a>
- Albini, A. & Monti, S. Photophysics and photochemistry of fluoroquinolones. *Chem Soc Rev* **32**, 238-250 (2003). <a href="https://doi.org:10.1039/b209220b">https://doi.org:10.1039/b209220b</a>
- Lorente, C., Capparelli, A. L., Thomas, A. H., Braun, A. M. & Oliveros, E. Quenching of the fluorescence of pterin derivatives by anions. *Photochem Photobiol Sci* **3**, 167-173 (2004). https://doi.org:10.1039/b313076b

- Jean, J. M. & Hall, K. B. 2-Aminopurine fluorescence quenching and lifetimes: Role of base stacking. *P Natl Acad Sci USA* **98**, 37-41 (2001). <a href="https://doi.org:DOI">https://doi.org:DOI</a> 10.1073/pnas.011442198
- O'Neill, M. A. & Barton, J. K. 2-Aminopurine: a probe of structural dynamics and charge transfer in DNA and DNA:RNA hybrids. *J Am Chem Soc* **124**, 13053-13066 (2002). https://doi.org:10.1021/ja0208198
- Jones, A. C. & Neely, R. K. 2-Aminopurine as a fluorescent probe of DNA conformation and the DNA-enzyme interface. *Q Rev Biophys* **48**, 244-279 (2015). https://doi.org:10.1017/S0033583514000158
- Lee, B. J., Barch, M., Castner, E. W., Jr., Volker, J. & Breslauer, K. J. Structure and dynamics in DNA looped domains: CAG triplet repeat sequence dynamics probed by 2-aminopurine fluorescence. *Biochemistry-Us* **46**, 10756-10766 (2007). https://doi.org:10.1021/bi7005674
- Neely, R. K., Magennis, S. W., Dryden, D. T. F. & Jones, A. C. Evidence of Tautomerism in 2-Aminopurine from Fluorescence Lifetime Measurements. *The Journal of Physical Chemistry B* **108**, 17606-17610 (2004). https://doi.org:10.1021/jp0490857
- Morel, A. C. *et al.* An aqua-adenine H-bonding interaction controlling the formation of the rare Zn(II)–N9(adenine) bond in crystal structure of diaqua(adenine)(iminodiacetato)zinc(II). *Inorganic Chemistry Communications* **6**, 1354-1357 (2003). <a href="https://doi.org/10.1016/j.inoche.2003.06.001">https://doi.org/10.1016/j.inoche.2003.06.001</a>
- Garcia-Teran, J. P. *et al.* Supramolecular architectures assembled by the interaction of purine nucleobases with metal-oxalato frameworks. Non-covalent stabilization of the 7H-adenine tautomer in the solid-state. *Dalton Trans*, 902-911 (2006). <a href="https://doi.org/10.1039/b510018f">https://doi.org/10.1039/b510018f</a>
- Mastropietro, T. F., Armentano, D., Marino, N. & De Munno, G. Metal–nucleobase interactions in magnesium(II) and manganese(II) complexes with adenine: Influence of the anion on the non-covalent stabilization of 7H-adenine tautomer. *Polyhedron* **26**, 4945-4954 (2007). <a href="https://doi.org/10.1016/j.poly.2007.06.037">https://doi.org/10.1016/j.poly.2007.06.037</a>
- Ai, H., Chen, J. & Zhang, C. Amino-imino adenine tautomerism induced by the cooperative effect between metal ion and H2O/NH3. *J Phys Chem B* **116**, 13624-13636 (2012). https://doi.org:10.1021/jp308937k
- Samijlenko, S. P., Krechkivska, O. M., Kosach, D. A. & Hovorun, D. M. Transitions to high tautomeric states can be induced in adenine by interactions with carboxylate and sodium ions: DFT calculation data. *J Mol Struct* **708**, 97-104 (2004). https://doi.org/10.1016/j.molstruc.2004.05.034
- Lakowicz, J. R. *Principles of fluorescence spectroscopy*. 2nd edn, (Kluwer Academic/Plenum, 1999).
- Yu, H. T., Colucci, W. J., McLaughlin, M. L. & Barkley, M. D. Fluorescence quenching in indoles by excited-state proton transfer. *J Am Chem Soc* **114**, 8449-8454 (1992). <a href="https://doi.org:10.1021/ja00048a015">https://doi.org:10.1021/ja00048a015</a>
- 45 Potyahaylo, A. L. & Hovorun, D. M. Various point contacts between neutral and deprotonated carboxylic groups of amino acids and 2-aminopurine. *Biopolym. Cell.* **18**, 351-354 (2002).
- Goncąlves, L. C. P. *et al.* Boosting photobioredox catalysis by morpholine electron donors under aerobic conditions. *Catalysis Science and Technology* **9**, 2682-2688 (2019). https://doi.org:10.1039/c9cy00496c

## **SUPPORTING INFORMATION**

# Buffer-Dependent Photophysics of 2-Aminopurine: Insights into Fluorescence Quenching and Excited-State Interactions

Souvik Poddar<sup>1,2</sup>, Marcia Levitus<sup>1,2,\*</sup>

# marcia.levitus@asu.edu

# **Table of Contents**

	Page
Materials and Sample Preparation	S2
Time Correlated Single Photon Counting: Instrumental Details	S2
Table S1 (Fluorescence quantum yields $(\phi_f)$ and lifetimes $(\tau)$ of 2AP and 2APr in HCl or NaOH solutions of various pH values)	S3
Figure S1: Absorbance and emission spectra of 2AP at various pH values (HCl or NaOH solutions)	S3
Table S2: Effect of NaCl concentration on the fluorescence quantum yield ( $\phi_f$ ) and lifetime ( $\tau$ ) of 2AP	S3
Table S3: Fluorescence quantum yields ( $\phi_f$ ) and lifetimes ( $\tau$ ) of 2AP in various buffer solutions	S4
Table S4: Fluorescence quantum yields $(\phi_f)$ and lifetimes $(\tau)$ of 2AP and 2APr in phosphate buffer solutions	S4
Figure S2: Fluorescence Spectra of 2APr and 2AP in 1M phosphate buffer at pH 5 and 9	S5
Figure S3: Fluorescence Spectra of 2APr and 2AP in 1M Carbonate buffer (pH 10), HEPES (pH 7), MOPS (pH 7) and TRIS-CI (pH 7.5)	S6
Figure S4: Fluorescence Intensity Decay of 2AP in 500 mM Phosphate buffer at pH 9	S6
Figure S5: Global Fit of the Fluorescence Intensity Decays of 2AP in 500 mM Phosphate buffer at pH 9.	S7
Analysis of the kinetic scheme of Fig. 6	S7
Figure S6	S8
Figure S7	S10
Figure S8	S10

<sup>&</sup>lt;sup>1</sup> School of Molecular Sciences, Arizona State University, 551 E. University Drive, Tempe, AZ, 85287, USA.

<sup>&</sup>lt;sup>2</sup> The Biodesign Institute Center for Single Molecule Biophysics, Arizona State University, Tempe, AZ, 85287, USA.

<sup>\*</sup> To whom correspondence should be addressed: ML Tel: +1-480-727-8586; Fax: +1-480-727-2378; Email:

#### **Materials and Sample Preparation**

#### Sources of Chemicals

- 2-amino purine (2AP): Millipore Sigma, #A3509-100MG.
- 2-amino purine riboside (2APr): AstaTech, #F12889.
- 3-(N-morpholino)propanesulfonic acid (MOPS): EMD Millipore Sigma, #475922-100GM.
- 4-(2-hydroxyethyl)-1-piperazineethanesulfonic acid (HEPES): Millipore Sigma, #H3375-25G.
- Tris(hydroxymethyl)aminomethane (TRIS base): VWR AMRESCO Life Science, #0826-1KG.
- Tris(hydroxymethyl)aminomethane hydrochloride (TRIS HCl): Fischer Scientific, #BP153-1.
- Deuterium oxide: Millipore Sigma, #151882-10X1ML.
- Potassium dideuterium phosphate: Millipore Sigma, #329916-1G.

All other chemicals (HCl, NaOH, NaCl, NaHCO<sub>3</sub>, Na<sub>2</sub>SO<sub>4</sub>, NaH<sub>2</sub>PO<sub>4</sub>, Na<sub>2</sub>HPO<sub>4</sub>) were obtained from various commercial sources.

#### **Buffers**

- 1M Phosphate buffer was prepared by mixing  $NaH_2PO_4$  and  $Na_2HPO_4$  in doubly distilled water at the ratio necessary to achieve the desired pH (5, 7, 9) (  $[NaH_2PO_4] + [Na_2HPO_4] = 1M$ ).
- 1M Carbonate buffer pH 10 was prepared by adding the amount of solid NaOH necessary to achieve pH 10 to a solution of NaHCO<sub>3</sub> prepared in doubly distilled water.
- 1M HEPES and 1M MOPS were prepared by adding the amount of solid NaOH necessary to achieve pH 7 to solutions of HEPES and MOPS prepared in doubly distilled water.
- 1 M TRIS-Cl was prepared by mixing TRIS base and TRIS HCl in doubly distilled water at the ratio necessary to achieve pH 7.5 ([TRIS] + [TRIS HCl] = 1 M).
- Solutions of NaCl and Na<sub>2</sub>SO<sub>4</sub> were prepared in doubly distilled water at the desired concentration.
- Solutions of Potassium dideuterium phosphate in  $D_2O$  were prepared the day of the experiment using a newly opened ampule of  $D_2O$ .

# **DNA** annealing

The ssDNA strands were annealed by adding equimolar amounts of each strand in the desired buffer and monitoring the reduction in 2AP fluorescence due to the formation of the double helix in real time. Annealing was considered complete when the 2AP fluorescence did not decrease further after the addition of an excess of the complementary strand. Samples were prepared in water, 20 mM phosphate, 50 mM phosphate, and 100 mM phosphate. The pH of all the buffers was 7. The final DNA concentration was ~12  $\mu$ M, which corresponded to a 2AP absorbance of ~0.08-0.1 at  $\lambda_{ex}$  = 310 nm.

### **Time Correlated Single Photon Counting: Instrumental Details**

Time-resolved fluorescence intensity measurements were performed using the time-correlated single-photon counting (TCSPC) technique. The excitation sources was a mode-locked Ti:Sapphire laser (Mira 900, Coherent) pumped by a frequency-doubled Nd:YVO4 laser (44% from an 18 W Verdi, Coherent). The 130 fs light pulses (at 800 nm with a repetition rate of 250 KHz) were generated by a regeneratively amplified Ti:S laser system (RegA 9000, Coherent Laser). The pulses were sent to an optical parametric amplifier (OPA) to generate the excitation light at 620 nm and then frequency-doubled to obtain excitation pulses at 310 nm. Fluorescence was collected at a 90° geometry and detected using a double-grating monochromator (Oriel Instruments) and a microchannel plate photomultiplier tube (Hamamatsu R3809U-51). A single-photon counting card (Becker-Hickel, SPC-830,  $2^{12}$  channels) was used for data acquisition.

Table S1: Fluorescence quantum yields ( $\phi_f$ ) and lifetimes ( $\tau$ ) of 2AP and 2APr in HCl or NaOH solutions of various pH values.

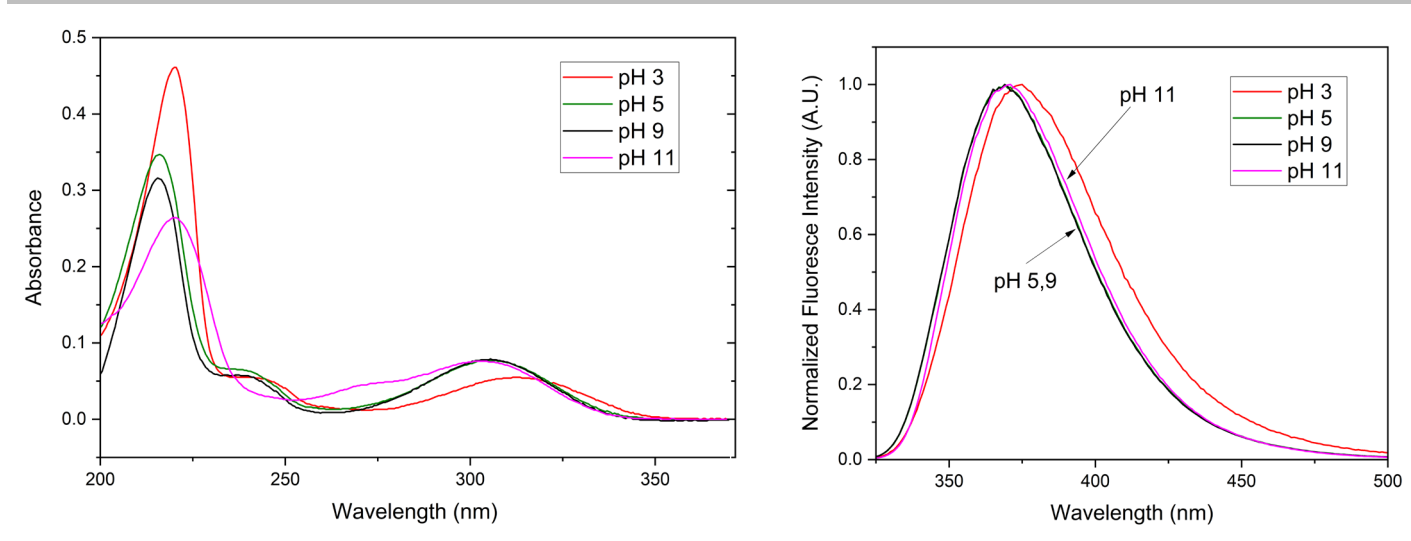
	2/	<b>AP</b>	2APr				
рН	ф <sub>f</sub> <sup>(а)</sup>	τ (ns)	фf	τ (ns)			
3	0.11	2.9 <sup>(b)</sup>	0.18	4.0 <sup>(c)</sup>			
4	0.44	11.2	0.53	10.1			
5	0.63	11.7	0.63	10.3			
6	0.68	11.6	0.64	10.3			
7	0.68	11.7	0.65	10.4			
8	0.68	11.6	0.63	10.3			
9	0.67	11.7	0.64	10.3			
10	0.69	11.6	0.63	10.3			
11	0.61	11.4	0.62	10.0			
14	0.006	N.D.	0.004	N.D			

(a) All values are relative to 2AP in water (see Materials and Methods)

N.D. = non determined

- (b) represents the amplitude average:  $\langle \tau \rangle = \sum_i a_i \tau_i$ . Three exponential terms were needed to fit the decay:  $a_1 = \sum_i a_i \tau_i$ . 0.66,  $a_2=0.04$ ,  $a_3=0.30$ ,  $\tau_1=0.06$  ns,  $\tau_2=1.05$  ns,  $\tau_3=9.30$  ns. (c) represents the amplitude average:  $\langle \tau \rangle = \sum_i a_i \tau_i$ . Two exponential terms were needed to fit the decay:  $a_1=0.06$  ns,  $a_2=0.04$ ,  $a_3=0.30$ ,  $a_3=0.30$ ,  $a_4=0.30$ ,  $a_5=0.30$ ,  $a_5=0.3$
- 0.55,  $a_2 = 0.45$ ,  $\tau_1 = 0.04$  ns,  $\tau_2 = 8.87$  ns.

Figure S1: Absorbance and emission spectra of 2AP at various pH values (HCl or NaOH solutions)



The concentration of all solutions used in the acquisition of absorption spectra were the same, and equal to 11.2 μM (assuming  $\varepsilon_{303} = 6,800 \text{ M}^{-1}\text{cm}^{-1}$  in water at pH 7)

Table S2: Effect of NaCl concentration on the fluorescence quantum yield ( $\phi_f$ ) and lifetime ( $\tau$ ) of 2AP

[NaCl] (mM)	φ <sub>f</sub> <sup>(a)</sup>	τ (ns)
50	0.68	11.7
100	0.69	11.7
250	0.68	N.D.
500	0.67	11.6
750	0.66	N.D.
1000	0.66	11.4

<sup>(</sup>a) All values are relative to 2AP in water (see Materials and Methods), N.D. = non determined

Table S3: Fluorescence quantum yields ( $\phi_f$ ) and lifetimes ( $\tau$ ) of 2AP in various buffer solutions

[Buffer] (mM)	Tris-Cl (pH 7.5)		MOPS (pH 7)		HEPES (pH 7		Carbonate (pH 10)					
	фf	τ (ns)	фf	τ (ns)	фf	τ (ns)	фf	$\langle  au  angle$ (ns) $^{ ext{(a)}}$	τ <sub>1</sub> (ns)	$\alpha_1$	τ <sub>2</sub> (ns)	
0	0.68	11.7	0.68	11.7	0.68	11.7	0.68	11.7	11.7	1	-	
50	0.65	11.2	0.60	10.8	0.51	9.4	0.47	8.4	8.4	1	-	
100	0.63	10.9	0.61	9.8	0.41	7.5	0.36	6.6	7.4	0.81	3.4	
200	0.59	10.4	N.D.	N.D.	N.D.	N.D.	N.D.	N.D.	N.D.	N.D.	N.D.	
250	0.58	10.2	0.45	7.9	0.27	5.0	0.21	3.9	4.8	0.68	2.0	
300	0.57	9.9	N.D.	N.D.	N.D.	N.D.	N.D.	N.D.	N.D.	N.D.	N.D.	
400	0.54	9.5	N.D.	N.D.	N.D.	N.D.	N.D.	N.D.	N.D.	N.D.	N.D.	
500	0.52	9.1	0.36	6.5	0.18	3.3	0.12	2.3	3.1	0.6	1.2	
750	0.44	8.3	0.27	N.D.	0.13	2.9	0.09	1.7	2.4	0.5	0.9	
1000	0.40	7.6	0.22	4.5	0.11	2.3	0.06	1.2	1.7	0.6	0.5	

N.D. = non determined, (a) Decays in carbonate buffer ( $\geq$  100 mM) are bi-exponential. Values of  $\alpha_2$  are not sown ( $\alpha_1$  +  $\alpha_2$  = 1).  $\langle \tau \rangle = \alpha_1 \tau_1 + (1 - \alpha_1) \tau_2$ 

Table S4: Fluorescence quantum yields ( $\phi_f$ ) and lifetimes ( $\tau$ ) of 2AP and 2APr in phosphate buffer solutions

	2AP									2APr						
	рŀ	15	рŀ	17			pH 9			рŀ	15	рŀ	17	pH 9		
[phosphate] (mM)	фf	τ (ns)	фf	τ (ns)	фf	〈τ 〉 (ns) <sup>(a)</sup>	τ <sub>1</sub> (ns)	$\alpha_1$	τ <sub>2</sub> (ns)	фf	τ (ns)	фf	τ (ns)	фf	τ (ns)	
0	0.63	11.7	0.68	11.7	0.67	11.7	11.7	1	N.D.	0.62	10.3	0.64	10.4	0.64	10.3	
50	0.48	7.7	0.41	6.6	0.39	6.7	6.7	1	N.D.	0.49	8.0	0.44	6.9	0.38	6.3	
100	0.35	5.7	0.29	5.4	0.28	5.01	6.5	0.38	4.08	0.39	6.5	0.33	5.3	0.28	4.6	
200	0.20	N.D.	0.17	3.3	0.17	3.1	6.6	0.08	2.82	N.D.	N.D.	N.D.	3.5	N.D.	N.D.	
250	0.19	3.3	0.16	3.0	0.15	2.9	4.9	0.23	2.33	0.24	4.3	0.19	3.3	0.15	2.7	
300	0.15	N.D.	0.13	2.5	0.13	2.4	3.5	0.25	2.01	N.D.	N.D.	N.D.	2.8	N.D.	N.D.	
400	0.12	N.D.	0.11	2.1	0.11	2.0	4.0	0.09	1.80	N.D.	N.D.	N.D.	2.3	N.D.	N.D.	
500	0.11	2.1	0.10	1.9	0.09	1.8	3.8	0.13	1.56	0.15	2.8	0.12	2.1	0.09	1.7	
750	0.07	1.6	0.08	1.5	0.07	1.4	2.7	0.14	1.18	0.11	2.2	0.09	1.7	0.07	1.3	
1000	0.06	1.3	0.06	1.3	0.06	1.2	2.1	0.15	1.05	0.08	1.8	0.08	1.4	0.06	1.1	

N.D. = non determined, (a) Decays are bi-exponential. Values of  $\alpha_2$  are not sown ( $\alpha_1 + \alpha_2 = 1$ ).  $\langle \tau \rangle = \alpha_1 \tau_1 + (1 - \alpha_1) \tau_2$ 

Figure S2: Fluorescence Spectra of 2APr and 2AP in 1M phosphate buffer at pH 5 and 9

Black lines: water. Red lines: 1M phosphate buffer.

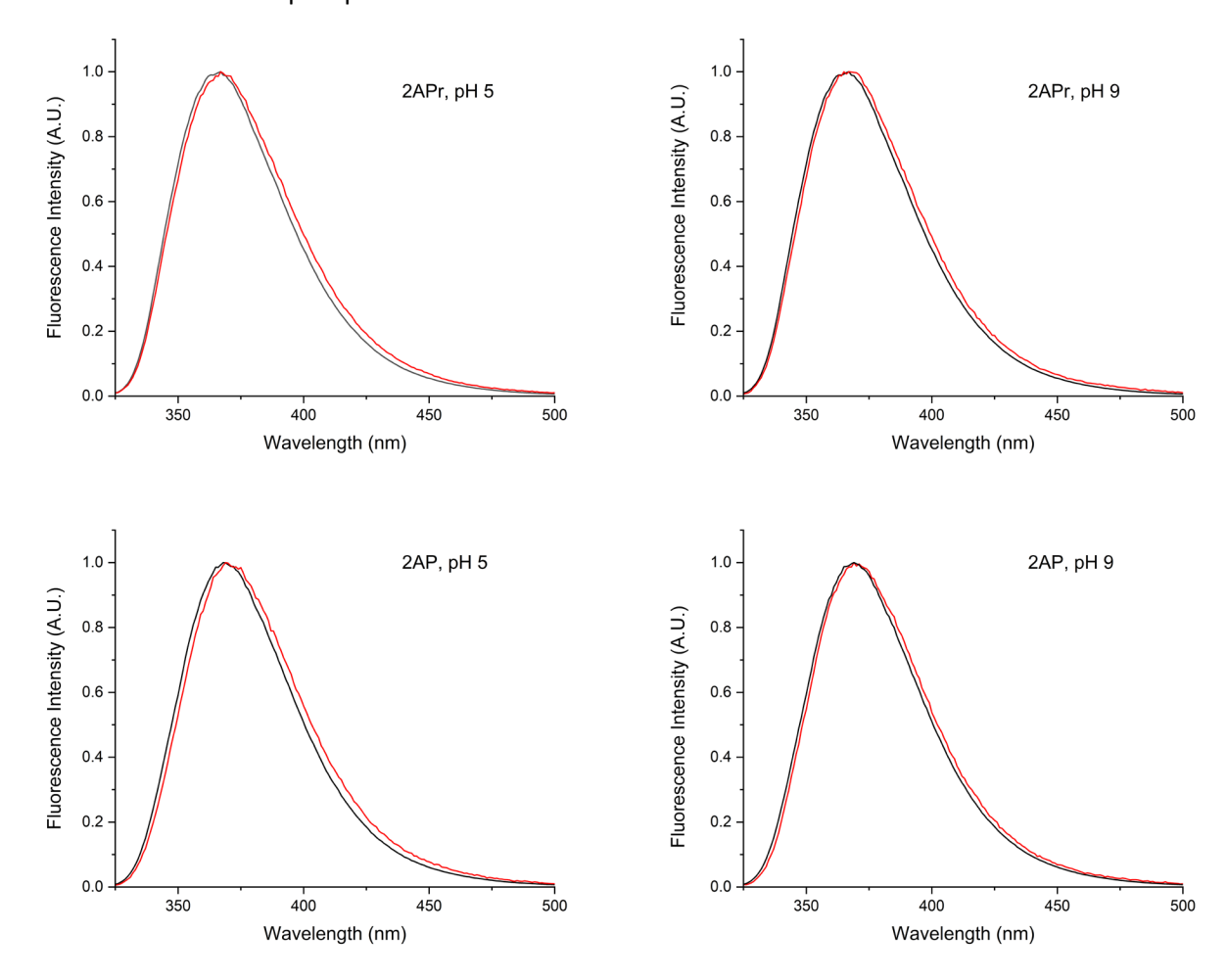


Figure S3: Fluorescence Spectra of 2APr and 2AP in 1M Carbonate buffer (pH 10), HEPES (pH 7), MOPS (pH 7) and TRIS-CI (pH 7.5)

Black lines: water. Red lines: 1M buffer.

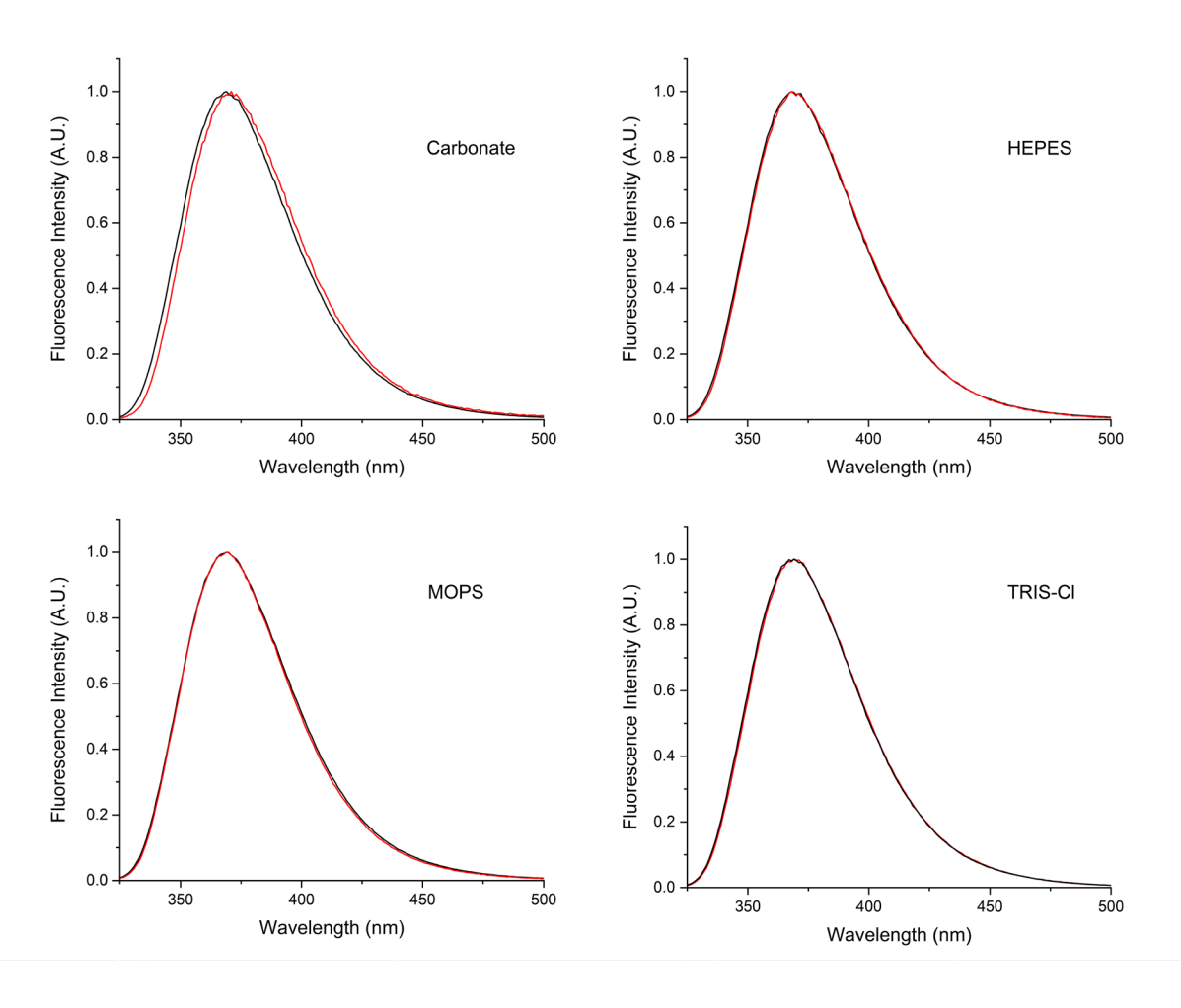


Figure S4: Fluorescence Intensity Decay of 2AP in 500 mM Phosphate buffer at pH 9

 $\lambda_{em}$  = 380 nm. Left: fit with one exponential term ( $\chi^2$  = 8.07). Right: fit with two exponential terms ( $\chi^2$  = 1.02, fitting parameters in Table S4). Red lines represent the fitted curve.

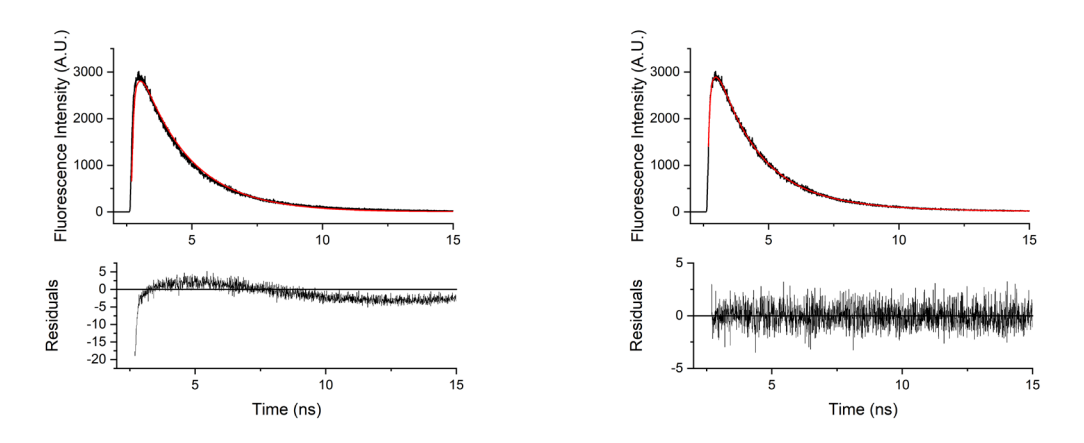
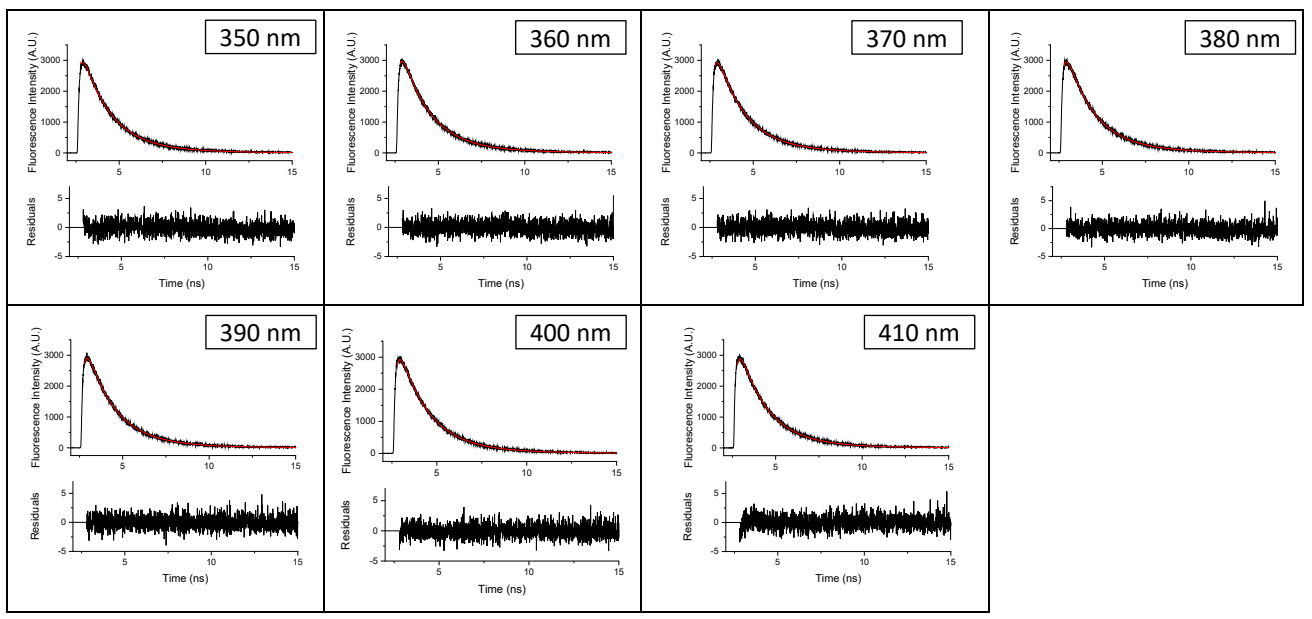


Figure S5: Global Fit of the Fluorescence Intensity Decays of 2AP in 500 mM Phosphate buffer at pH 9.



Seven decays were measured in the  $\lambda_{\rm em}$  = 350-410 nm range and fitted simultaneously with two exponential terms using the equation  $I(t,\lambda_{em})=A_1(\lambda_{em})e^{-t/\tau_1}+A_2(\lambda_{em})e^{-t/\tau_2}$ .

 $\lambda_{\text{ex}}$  = 310 nm in all cases. The lifetimes,  $\tau_1$  and  $\tau_2$ , are assumed to be common among all decay curves. The amplitudes shown in Table 3 ( $\alpha_i(\lambda_{em})$ ) were calculated from the pre-exponential factors ( $A_{1,2}(\lambda_{em})$ ) as  $\alpha_{1,2}(\lambda_{em}) = \frac{A_{1,2}(\lambda_{em})}{A_1(\lambda_{em})+A_2(\lambda_{em})}$ .

The resulting  $\chi^2$  was 1.07

## Analysis of the kinetic scheme of Fig. 6

The differential equations for the decay of the excited states of free 2AP (A\*) and 2AP complexed with phosphate (B\*) are:

$$-\frac{d[A^*]}{dt} = (k_A + k_1[P])[A^*] - k_2[B^*]$$
 Eq. S1 
$$-\frac{d[B^*]}{dt} = (k_2 + k_B)[B^*] - k_1[P][A^*]$$

Integration of these equations with  $[A^*] = [A^*]_0$  and  $[B^*] = 0$  at t = 0 yields

$$[A^*](t) = \frac{[A^*]_0}{\gamma_1 - \gamma_2} [(X - \gamma_2)e^{-t\gamma_1} + (\gamma_1 - X)e^{-t\gamma_2}]$$
 Eq. S2

$$[B^*](t) = rac{[A^*]_0}{\gamma_1 - \gamma_2} k_1[P][e^{-t\gamma_2} - e^{-t\gamma_1}]$$
 Eq. S3

where

$$\gamma_1 = \tau_1^{-1} = \frac{1}{2}(X + Y + W)$$
 Eq. S4

$$\gamma_2 = \tau_2^{-1} = \frac{1}{2}(X + Y - W)$$
 Eq. S5

$$X = k_A + k_1[P]$$
 Eq. S6

$$Y = k_B + k_2$$
 Eq. S7

$$W = \left[4k_2k_1[P] + (Y - X)^2\right]^{1/2}$$
 Eq. S8

The fluorescence decays of A and B at wavelength  $\lambda_{em}$  are given by

$$I_A(\lambda_{em}, t) = \alpha_1(\lambda_{em})e^{-t/\tau_1} + \alpha_2(\lambda_{em})e^{-t/\tau_2}$$
 Eq. S9 = Eq. 2

$$I_B(\lambda_{em}, t) = \beta_1(\lambda_{em})e^{-t/\tau_1} + \beta_2(\lambda_{em})e^{-t/\tau_2}$$
 Eq. S10 = Eq. 3

and depend on the concentrations of the corresponding excited states,  $[A^*](t)$  and  $[B^*](t)$  as

$$I_A(\lambda_{em},t) = \Gamma_A.F_A(\lambda_{em})[A^*](t)$$
 Eq. S11

$$I_B(\lambda_{em},t) = \Gamma_B.F_B(\lambda_{em})[B^*](t)$$
 Eq. S12

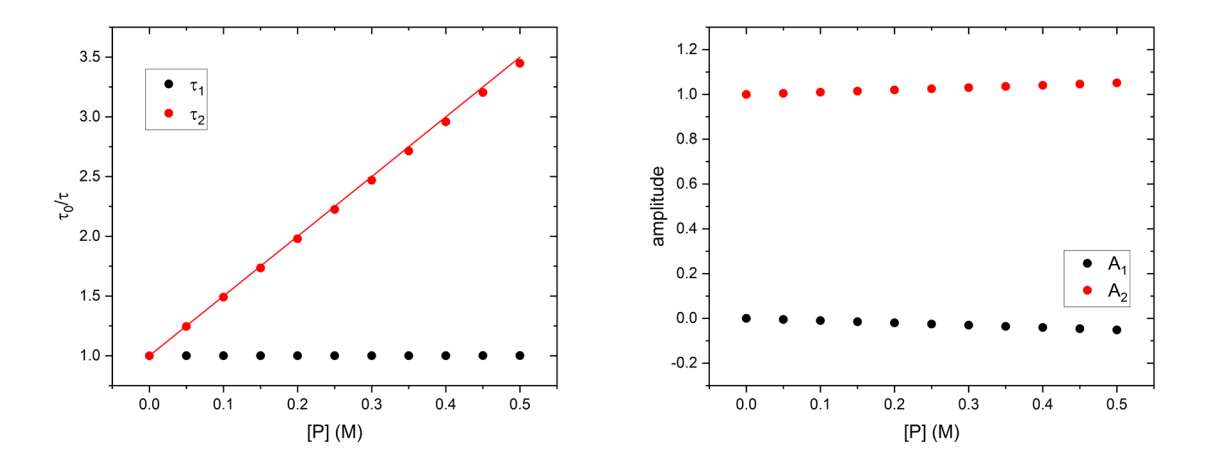
Here,  $\Gamma_A$  and  $\Gamma_B$  represent the radiative decay rates, and  $F_A(\lambda_{em})$  and  $F_B(\lambda_{em})$  are the spectral emission contours (spectral shapes) normalized to unit area. The values of  $k_A$  and  $k_B$  are related to the radiative decay rates through the corresponding fluorescence quantum yields:  $\Gamma_A = \phi_A k_A$ ,  $\Gamma_B = \phi_B k_B$ .

#### Figure S6

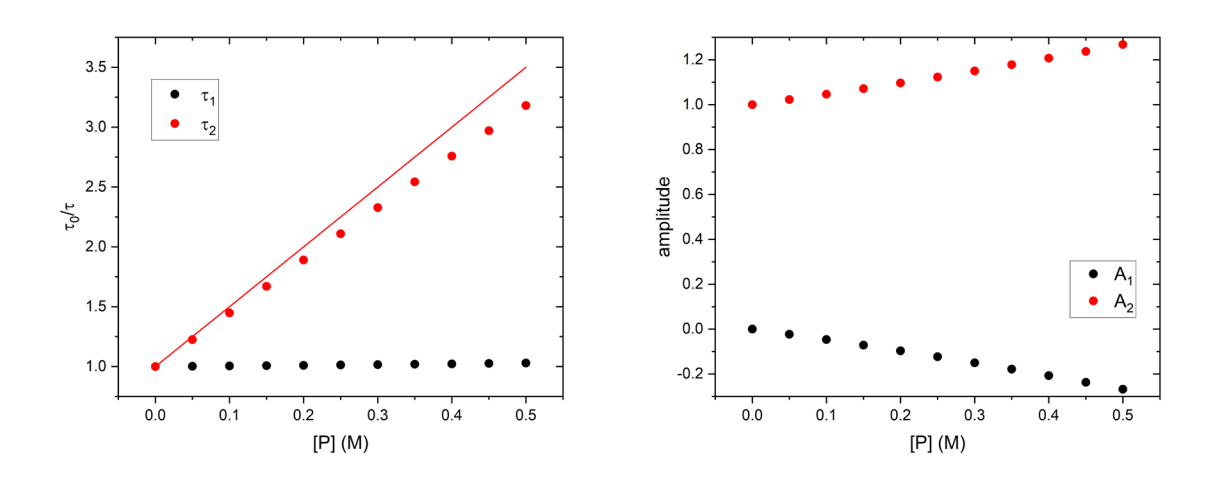
Expected Stern-Volmer plots and pre-exponential amplitudes ( $A_1$ ,  $A_2$ ) for a single species "A" that interacts with a quencher (e.g. phosphate, P) in the excited state according to the mechanism of Fig. 6. Fluorescence decays ( $I_T(\lambda_{em},t)=A_1e^{-t/\tau_1}+A_2e^{-t/\tau_2}$ ) were calculated according to Eq. 10 using  $\Gamma_A=\Gamma_B=10^8s^{-1}$ ,  $k_1=5\times10^8M^{-1}s^{-1}$ ,  $\phi_A=1$ ,  $[A^*]_0=1$  and values of  $k_2$  and  $\phi_B$  as indicated in each case. The red solid lines represent the function  $\tau_0/\tau=1+(k_1/k_A)[P]$ , where [P] is the concentration of quencher.

Case I:  $k_2 = 1 \times 10^8 s^{-1} \phi_B = 0.02$ .

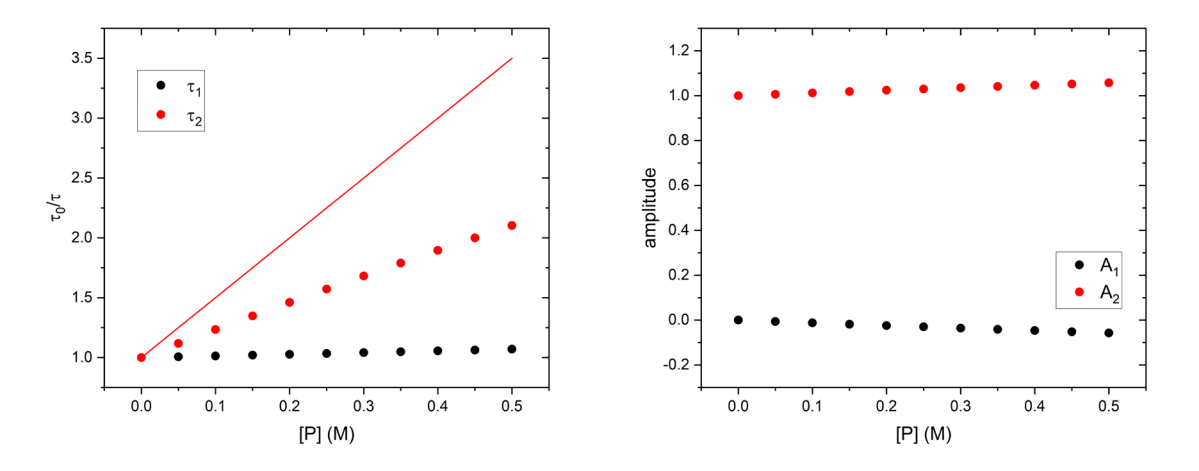
Calculated lifetimes at [P] = 0 are  $\tau_{0,1}=0.196~ns$  and  $\tau_{0,2}=10.0~ns$ . The short lifetime does not depend on [P] and has a negligible amplitude at all [P] values. Results are indistinguishable from a simple dynamic mechanism (solid line).



**Case II**:  $k_2 = 1 \times 10^8 s^{-1} \ \phi_B = 0.1$ . Calculated lifetimes at [P] = 0 are  $\tau_{0,1} = 0.909 \ ns$  and  $\tau_{0,2} = 10.0 \ ns$ . The short lifetime does not depend on [P] but has a significant negative amplitude at high [P] values.



Case III:  $k_2=1\times 10^9 s^{-1}$   $\phi_B=0.1$ . Calculated lifetimes at [P] = 0 are  $\tau_{0,1}=0.5~ns$  and  $\tau_{0,2}=10.0~ns$ . The short lifetime does not depend on [P] and has a negligible amplitude at all [P] values. Results are indistinguishable from a simple dynamic mechanism but with an apparent Stern-Volmer constant that does not equal  $k_1k_A^{-1}$  (red line).



Page S9

# Figure S7

Stern-Volmer plots of 2AP quenched by  $H_2PO_4^-$  or  $D_2PO_4^-$ . Left: Fluorescence quantum yields. Right: Fluorescence lifetimes.

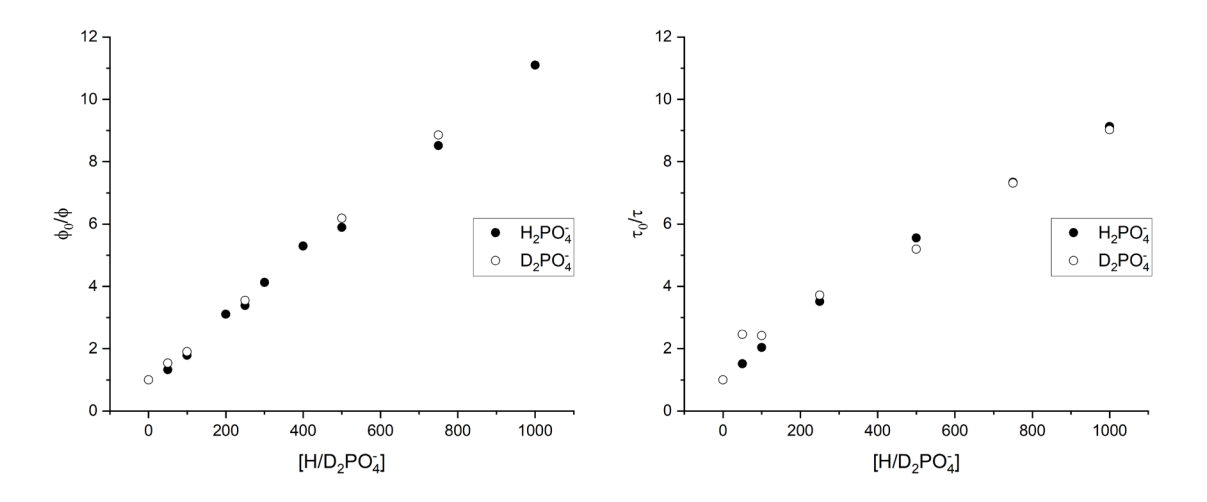


Figure S8

Schematic representation of the interactions between Na<sup>+</sup>, CH<sub>3</sub>COO<sup>-</sup> and the 7H-adenine tautomer according to the calculations of Samijlenko et al. (*J Mol Struct* **708**, 97-104 (2004)). The 7H proton is transferred from the adenine base to the acetate ion (indicated with an arrow).

